



ELSEVIER

Contents lists available at ScienceDirect

Journal of Magnetism and Magnetic Materials

journal homepage: www.elsevier.com/locate/jmmm

Planar steering of a single ferrofluid drop by optimal minimum power dynamic feedback control of four electromagnets at a distance

R. Probst, J. Lin, A. Komae, A. Nacev, Z. Cummins, B. Shapiro*

Fischell Department of Bioengineering, 1226 Kim Building, University of Maryland, College Park, MD 20742, USA

ARTICLE INFO

Article history:

Received 10 March 2010

Received in revised form

2 August 2010

Keywords:

Magnetic particle

Magnetic carrier

Nanoparticle

Ferrofluid

Magnetic drug delivery

Manipulation at a distance

Control

Feedback

Electromagnet

Dielectrophoresis

ABSTRACT

Any single permanent magnet or electromagnet will always attract a magnetic fluid. For this reason it is difficult to precisely position and manipulate ferrofluid at a distance from magnets. We develop and experimentally demonstrate optimal (minimum electrical power) 2-dimensional manipulation of a single droplet of ferrofluid by feedback control of 4 external electromagnets. The control algorithm we have developed takes into account, and is explicitly designed for, the nonlinear (fast decay in space, quadratic in magnet strength) nature of how the magnets actuate the ferrofluid, and it also corrects for electromagnet charging time delays. With this control, we show that dynamic actuation of electromagnets held outside a domain can be used to position a droplet of ferrofluid to any desired location and steer it along any desired path within that domain—an example of precision control of a ferrofluid by magnets acting at a distance.

© 2010 Elsevier B.V. All rights reserved.

1. Introduction

We consider an initial ferrofluid control problem: the precise manipulation of a single drop of ferrofluid by four external electromagnets. Precision control is achieved by feedback: we sense the location of the droplet by a camera and imaging software and then correctly actuate the electromagnets at each time to move it from where it is to closer to where it should be (Fig. 1). Repeating this magnetic correction at each time quickly forces the droplet to the desired stationary or moving target and allows us to precisely control its position over time.

Control design, the mathematical development of the algorithm that determines how to turn on the magnets to create the needed position correction at each time, is challenging. It is recognized that each magnet can only pull the fluid towards it; any single magnet cannot push a magnetic fluid [1,2]. Further, the available pulling force drops rapidly with the ferrofluid distance from each magnet [3] (see Fig. 2 and our derivation in Appendix 3.1 in the supplementary material (doi:10.1016/j.jmmm.2010.08.024)). This makes it difficult to move a ferrofluid droplet left when it is close to the rightmost magnet (the other three magnets must pull it from a long distance, and not over-pull it once it

approaches them). Our control algorithm accounts for these difficulties, both for the pulling-only nature of each magnet and for the rapid drop-off in magnetic force with distance, and it does so in an optimal (minimal electrical power) and smooth fashion. This is done by first find the set, or manifold, of all electromagnet actuations that will create the desired droplet motion, and then within this manifold picking the minimum power solution. Significant effort has been devoted to insuring that the numerical computations of the optimum are accurate and robust, and a sophisticated nonlinear filter has been integrated into the control to yield smooth magnet actuations that can be implemented experimentally. Our method takes into account the electromagnet strength limitations and it corrects for electromagnet dynamics, their charging time lag, by a high-pass temporal filter inserted into the control loop. These innovations provide a scalable control method that can be extended to larger and stronger magnets in the future.

Our interest here is to enable strong magnets to manipulate magnetic particles to deeper targets [4–7]. As such, we are interested in control algorithms that optimally exploit the capabilities of bigger magnets and that account for their charging time delays. We believe that the algorithms we have designed and demonstrated here can be scaled up to high strength magnets. Compared to our prior work of manipulating single [8,9] and multiple particles [10] by electric fields and electroosmotic flows [11,12], which can both pull and push particles, the specific

* Corresponding author. Tel.: +1 301 405 4191; fax: +1 301 405 9953.
E-mail address: benshap@umd.edu (B. Shapiro).

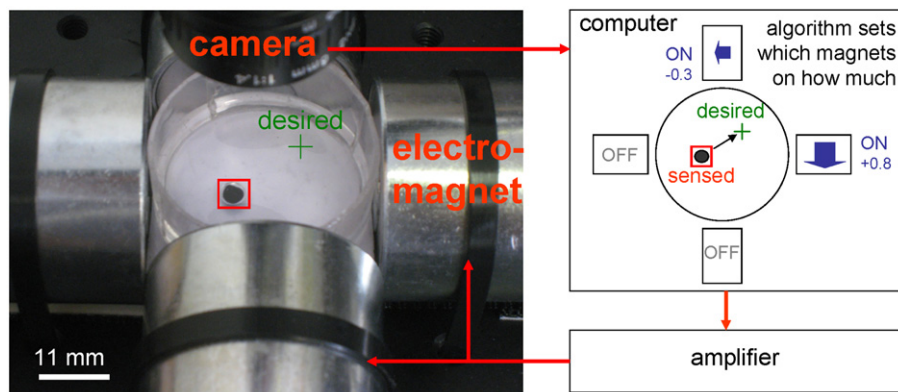


Fig. 1. Feedback control of 4 electromagnets can accurately steer a single ferrofluid droplet along any desired path and hold it at any location. Here a camera, computer, amplifier, and the 4 electromagnets are connected in a feedback loop around a petri dish containing a single droplet of ferrofluid. The camera observes the current location of the droplet; the computer, using the optimal nonlinear control algorithm developed below, computes the electromagnet actuations required to move the droplet from where it is to where it should be; and the amplifier applies the needed voltages to do so. This loop repeats at each time to steer the droplet.

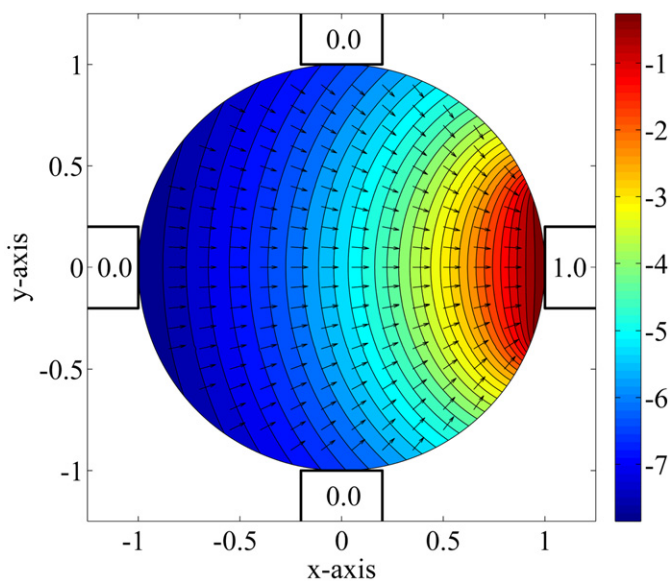


Fig. 2. The magnetic field created by the first magnet and the resulting force on a superparamagnetic particle at any location in the petri dish. The plot is colored by the magnetic field intensity squared on a log scale ($\log|H^2|$), and the resulting force directions, according to Eq. (4) below, are shown by the black arrows at each location. The particle is always attracted to regions of highest magnetic field intensity, i.e. here to the on right magnet. (This, and subsequent theory plots, are shown in non-dimensional variables and magnetic strength units for simplicity of presentation).

challenges that arise for magnetic control of a single ferrofluid droplet with larger magnets are as follows. (1) The pull only nature of the magnetic actuation. (2) The sharp drop-off in magnetic force with distance from the magnet: applying a needed magnetic field, when the droplet is far away, can easily and dramatically over-pull the droplet as it gets slightly closer to that magnet. (3) The maximum strength constraints of the magnets, which provide a hard stop to the amount of control authority available. This makes the minimum electrical power control both reasonable and desirable, (4) The nonlinear cross-coupling between magnets (turning on two magnets at once is not the same as the sum of turning on each magnet individually). A control law based on single magnet actuations will have degraded performance on the diagonals between magnets. Our method

works effectively over the entire spatial domain. (5) The related need to switch magnet actuation smoothly in time from one set of magnets to another as the ferrofluid droplet moves through its domain (our control design achieves this). (6) The need to correct for electromagnet coil charging time delays. This last aspect is crucially important for deeper control using larger and stronger magnets that will have longer charging times.

Design and demonstration of control algorithms for minimum power precision control of magnetic particles and fluids are also relevant for magnetofection [13], single particle manipulation (magnetic tweezers) [14–17], lab-on-a-chip systems that include magnetic particles or fluids [18,19], as well as magnetic drug delivery [20–31]. Magnetofection, the delivery of magnetic particles into cells by an applied magnetic force, could benefit from the approach described here—our technique could be used to position a droplet of magnetic particles above a small region of target cells, and then a magnetic field applied at the bottom could draw the particles into those target cells only. For magnetic particle manipulation, or magnetic tweezers, our method shows how to achieve precision control with the lowest possible electromagnetic powers, thus allowing micro-fabricated magnets [16,19,32–36], which have a practical limit on how big a magnetic field they can produce, to be placed further apart and to control magnetic particles over a larger spatial domain. Since magnetic tweezing forces scale with particle volume [35,37], minimum power control should allow more effective manipulation of smaller objects since it will enable the available magnets to create manipulation forces more efficiently. Our control results could also benefit dielectrophoresis [38–40] lab-on-a-chip microfluidic applications. DEP and magnetic actuation share the same governing equations for the force on the actuated object (replace the magnetic field \vec{H} in Eq. (7) by the electric field \vec{E}). Thus the mathematics presented here applies equally to DEP control. Our optimal algorithm could allow each standard 4-electrode DEP pad to steer a single object, with minimum electrical power.

Past work in control of magnetic particles and magnetizable objects has included magnetically assisted surgical procedures, MRI control of ferromagnetic cores and implantable robots, ferrofluid droplet levitation, magnetic tweezers, and nanoparticle magnetic drug delivery in animal and human studies. Methods to manipulate a rigid implanted permanent magnet through the brain with a view to guide the delivery of hyperthermia to brain tumors are presented in [41,42]. Here a point-wise optimization is stated for the magnetic force on the implant and example numerical solutions are shown, which displays jumps and

singularities similar to the ones we had to overcome in this work. Based on market opportunities, the focus of this group changed to magnetically assisted cardiovascular surgical procedures and led to the formation of the company Stereotaxis (www.stereotaxis.com/). This company now uses magnetic control to guide catheters, endoscopes, and other tools with magnetic tips for precision treatment of cardiac arrhythmias and other cardiovascular interventions. Stereotaxis catheter control algorithms are not disclosed completely but are noted briefly in published patents [43–48]. Control of magnetizable devices and ferromagnetic cores using an MRI machine as the actuator are presented by Martel et al. [49], Mathieu et al. [50], and Tamaz et al. [51], who also discuss manipulation of implantable magnetic robots [52–54] and magnetic guidance of swimming magnetotactic bacteria [55,56].

In terms of feedback control of microscopic and nanoscopic magnetizable objects, in [57] a ferrofluid is levitated by feedback control of a single upright electromagnet. Here the droplet of nanoparticles is passively attracted to the electromagnets' vertical axis and active feedback is used to modulate the strength of the magnet to stabilize the drop up and down against gravity and disturbances. Two- and three-dimensional control of magnetic particles in microscopic devices (magnetic tweezers) is described in [14–17,34,37], including magnet design and feedback control methods that enable impressively precise and sensitive capabilities for manipulating magnetic microscopic objects [35,58]. Finally, prior work in magnetic manipulation of therapeutic ferromagnetic nanoparticles (magnetic drug delivery) has progressed to animal and human clinical trials [20,21,27,31,59]. Magnetic manipulation here is currently limited to static magnets, either held externally [60–65] or implanted [66–71]—as yet there is no active feedback control in this arena.

Compared to prior work, our research here is focused on optimal control for minimum power smooth and deep manipulation of a ferrofluid, with a view towards enabling feedback control of magnetic drug delivery to reach deeper tumors in the long term (see also [4,5,7]). To this end, we have addressed the next major step: we have developed and experimentally demonstrated a novel and sophisticated optimal control algorithm to effectively manipulate a single ferrofluid droplet by feedback control. This algorithm was explicitly designed to address the highly nonlinear and cross-coupled nature of dynamic magnetic actuation and to best exploit available electromagnetic forces.

2. Theory and Modeling

Magnetic fields are described by Maxwell's equations [72]. In our case, we are changing magnetic fields slowly (compared to radio frequencies); thus the magneto-static equations are appropriate. These are

$$\nabla \vec{H} = \vec{j}, \quad (1)$$

$$\nabla \vec{B} = 0, \quad (2)$$

$$\vec{B} = \mu_0(\vec{H} + \vec{M}) = \mu_0(\vec{H} + \chi \vec{H}), \quad (3)$$

where \vec{B} is the magnetic field (tesla), \vec{H} is the magnetic intensity (amperes/meter), \vec{j} is the current density (A/m²), \vec{M} is the material magnetization (A/m), χ is the magnetic susceptibility, and $\mu_0 = 4\pi \times 10^{-7}$ N/A² is the permeability of vacuum. These equations hold true in vacuum and in materials (in air and liquid), for permanent magnets (magnetization $\vec{M} \neq 0$) and for electromagnets (current $\vec{j} \neq 0$). For our simple petri dish

surrounded by four electromagnets configuration, these equations can be readily solved using MATLAB.

The force on a single superparamagnetic particle is then [7,26,73,74]

$$\vec{F}_M = \frac{2\pi a^3}{3} \frac{\mu_0 \chi}{1 + \chi/3} \nabla \|\vec{H}\|^2 = \frac{4\pi a^3}{3} \frac{\mu_0 \chi}{1 + \chi/3} \left(\frac{\partial \vec{H}}{\partial \vec{x}} \right)^T \vec{H}, \quad (4)$$

where a is the radius of the particle (m), ∇ is the gradient operator (with units 1/m), and $\partial \vec{H} / \partial \vec{x}$ is the Jacobian matrix of \vec{H} with respect to the position vector $\vec{x} = (x, y, z)$. The first relation states that the force on a single particle is proportional to the gradient of the magnetic field intensity squared—i.e. a superparamagnetic particle will always experience a force from low to high applied magnetic field; it will be attracted to any single turned-on magnet regardless of its polarity. The second relation, which is obtained by applying the chain rule to the first one, is more common in the literature and clearly shows that a spatially varying magnetic field ($\partial \vec{H} / \partial \vec{x} \neq 0$) is required to create a magnetic force.

If the applied magnetic field is sufficient to magnetically saturate the particle, then $(\partial \vec{H} / \partial \vec{x})^T \vec{H}$ in Eq. (4) is modified to $(\partial \vec{H} / \partial \vec{x})^T \vec{M}_{sat}$, where \vec{M}_{sat} is the saturated magnetization of the particle. Since \vec{M}_{sat} lines up with \vec{H} , this does not change the direction of the force, only its size. In our case, the applied magnetic field never reaches the saturation limit of our particles and so Eq. (4) is correct as stated for any single magnetic particle.

When a magnetic force is applied, a single particle will accelerate in the direction of that force until it sees an equal and opposite fluid (Stokes) drag force. Since the Stokes force is [75–77]

$$\vec{F}_S = -6\pi a \eta \vec{v}, \quad (5)$$

where \vec{v} is the velocity of the particle relative to the fluid. Our nanoparticles are suspended in a solution of deionized water. During the experiments, we place them on top of a layer of high viscosity mineral oil (to keep the particles suspended and limit particle interactions with the bottom of the petri dish although the ferrofluid does still sink slowly and eventually does touch the petri dish surface). Thus, for us, the relevant surrounding fluid is the mineral oil and it has a viscosity of $\eta = 0.0576$ kg/(m s). Now, setting Eq. (5) equal to Eq. (4) and solving for velocity, we get

$$\vec{v}_{ss} = \frac{a^2}{9\eta} \frac{\mu_0 \chi}{1 + \chi/3} \nabla \|\vec{H}\|^2 = k \nabla \|\vec{H}\|^2, \quad (6)$$

where $k = a^2 \mu_0 \chi / 9\eta(1 + \chi/3)$ is the magnetic drift coefficient ($k \approx 1.6 \times 10^{-20}$ m⁴/A² s for our 100 nm diameter particles). This steady state velocity is achieved very quickly. For our particles it is predicted to be achieved in nanoseconds (the time constant is computed from Newton's second law by comparing the nanoparticle mass times acceleration versus the velocity dependent Stokes drag force).

We manipulate a single droplet of ferrofluid, which is composed of many superparamagnetic nanoparticles held together by surface tension and magnetic interactions. The net force on the droplet, and hence its resulting velocity, is still in the direction of $\nabla \|\vec{H}\|^2$ as in Eqs. (4) and (6). The issue now is the magnitude of that velocity due to particle-to-particle interactions. Analogously to Eq. (6), we define k' as the magnetic drift coefficient for the entire ferrofluid droplet

$$\vec{v}_{droplet,ss} = k' \nabla \|\vec{H}\|^2. \quad (7)$$

To quantify k' , we measured droplet velocities under the action of a single magnet for two droplet volumes of 5 and 7.5 μ L and compared them to theoretical predictions (see Appendix 3.1, doi:10.1016/j.jmmm.2010.08.024). The predicted motion best matched the observed motion, for the majority of the droplets

trajectory, when $k' \approx 3.5 \times 10^{-13}$ and $k' \approx 4.2 \times 10^{-13} \text{ m}^4/\text{A}^2 \text{ s}$ for the two droplet sizes, respectively. However, the speed of the motion was under-predicted at the end of the trajectory when the droplet quickly snapped to the edge of the petri dish within the high-field region of the turned-on external magnet (Figure SM-3 in the supplementary material appendix, doi:10.1016/j.jmmm.2010.08.024).

Four scenarios were considered to understand and qualitatively explain the difference between the magnetic drift coefficient predicted for a single particle and that inferred for the ferrofluid droplet: (1) the motion of a single nanoparticle, (2) the motion of a chain of particles held together by magnetic particle-to-particle interactions, (3) the motion of an agglomerate of particles held together by magnetic particle-to-particle and chain-to-chain interactions, and (4) the motion of a rigid ferromagnetic bead of the size of the droplet (corresponding to the case, where all the particles in the droplet are held together and all act as one mass). Overall, the third option best explained the observed k' values. Options 1 and 4 dramatically under-predicted and modestly over-predicted k' , respectively. The force on single chains of particles (second option), including a chain of the entire length of the droplet, was also not enough to account for the measured k' values. Only the third option could explain the measurements and was consistent with prior studies on particle-to-particle interactions which showed that particles can form chains and superstructures that dramatically increase the net magnetic force compared to the net viscous drag [78–82]. This explanation is also compatible with our finding that the magnetic drift coefficient varies and is greatest when the droplet is in the high field region near the turned-on magnet: the higher magnetic field increases chaining and superstructures.

We note that our control performance is insensitive to the value of k' —it continues to work even if we do not know k' accurately and do not account for its variation with the local magnetic field strength. This is because the control always applies a velocity to move the droplet from where it is towards where it should be—it needs only to set the direction correctly, the magnitude of the velocity is not critically important since another correction will occur at the next time step. Further, the variation in k' is only appreciable at the edges of the petri dish closest to the external magnets; k' is close to constant for the majority of the petri dish interior.

Based on the above, we now state the motion of the droplet as a function of the actuation of the four magnets—this is information we need to know in order to design the magnets control law. Let $\vec{H}_1(x,y)$, $\vec{H}_2(x,y)$, $\vec{H}_3(x,y)$, and $\vec{H}_4(x,y)$ be the magnetic fields in the xy plane, across the petri dish, when each magnet is turned on with a 1 A current. The first magnetic field $\vec{H}_1(x,y)$ is shown in Fig. 2 as computed by MATLAB, the other three \vec{H}_k 's are 90° rotations of \vec{H}_1 . Let u_1 , u_2 , u_3 and u_4 be the instantaneous electrical current in each of the four magnets, respectively. Then, by the linearity of the magneto-static Eqs. (1)–(3), the time-varying magnetic field that we apply is given by

$$\vec{H}(x,y,t) = u_1(t)\vec{H}_1(x,y) + u_2(t)\vec{H}_2(x,y) + u_3(t)\vec{H}_3(x,y) + u_4(t)\vec{H}_4(x,y). \quad (8)$$

In our experiments, we checked that this superposition of magnetic fields is valid. The concern was that the magnetic field from one magnet could perturb the core of another magnet. We measured the magnetic field in the petri dish due to the action of one magnet only, due to the action of another magnet only, and when they were both turned-on together. We found that the magnetic field due to both magnets was exactly equal to the sum of the magnetic field due to each magnet turned-on alone. The

explanation for this is that the magnets are sufficiently far apart, and the magnetic fields that they produce fall off sufficiently quickly, so that one magnet cannot substantially change the magnetization of the core of another magnet.

During feedback control, we do not have direct access to the vector of currents $\vec{u}(t) = [u_1(t) \ u_2(t) \ u_3(t) \ u_4(t)]^T$ because we cannot instantaneously charge a magnet to any desired strength. Instead, we control the vector of voltages $\vec{V}(t) = [V_1(t) \ V_2(t) \ V_3(t) \ V_4(t)]^T$. To first order, the current in each magnet is related to its voltage by simple time delay dynamics [83]. In vector form, this voltage-current relationship for all the magnets is given by

$$\frac{d}{dt} \vec{u}(t) = -\frac{R}{L} \vec{u}(t) + \frac{1}{L} \vec{V}(t), \quad (9)$$

where R and L are the resistance and inductance of the magnets, respectively. Our control corrects for this time delay by a specially designed nonlinear temporal filter.

Substituting Eq. (8) into the ferrofluid droplet velocity Eq. (7) gives the final model for the droplet motion in terms of the applied control

$$\begin{aligned} \frac{d}{dt} [x(t) \ y(t)] &= k' \nabla \left\| \sum_{i=1}^4 u_i(t) \vec{H}_i(x,y) \right\|^2 \\ &= k' \sum_{j=1}^4 \sum_{i=1}^4 u_i(t) [\nabla (\vec{H}_i(x,y) \cdot \vec{H}_j(x,y))] u_j(t) \\ &= k' [\vec{u}^T(t) P_x(x,y) \vec{u}(t) \ \vec{u}^T(t) P_y(x,y) \vec{u}(t)], \end{aligned} \quad (10)$$

where $[x(t) \ y(t)]$ is the current location of the droplet in the petri dish; the second equality was achieved by carrying out the square, by multiplying $\vec{H} = u_1 \vec{H}_1 + u_2 \vec{H}_2 + u_3 \vec{H}_3 + u_4 \vec{H}_4$ by itself and then moving the gradient operator into the resulting double summation, and the last equality is a compact matrix representation with subscript T denoting vector transpose and the matrices P_x and P_y defined as

$$\begin{aligned} P_x(x,y) &= [\partial (\vec{H}_i(x,y) \cdot \vec{H}_j(x,y)) / \partial x]_{4 \times 4}, \\ P_y(x,y) &= [\partial (\vec{H}_i(x,y) \cdot \vec{H}_j(x,y)) / \partial y]_{4 \times 4}. \end{aligned} \quad (11)$$

All other variables are as defined previously. Together with Eq. (9), this is the model for droplet's motion as a function of the applied control. It is a nonlinear differential equation—the P matrices depend on the droplet's location, since the magnetic field applied by each magnet varies in space across the petri dish. The dynamics is quadratic in the current control vector \vec{u} because the force depends on the gradient of the magnetic field squared. This means the droplet's motion depends on both single magnet actuation and on $u_i u_j$ cross terms—the velocity created by turning on two magnets at the same time is not the sum of the velocities created by each magnet alone. Our control is explicitly designed to account for this quadratic nature of the dynamics.

3. Quadratic model-based control

Our control operates by continuously directing the ferrofluid droplet from where it is measured to be towards where it should go (Fig. 1). With this approach, we can both hold the ferrofluid at a target location (the control continually puts it back) and we can steer the droplet along the desired trajectories (the control is always moving the droplet towards its next desired location). At each time we compute a displacement error vector between the droplet's desired and measured position $\vec{d} = \vec{x}_{\text{desired}} - \vec{x}_{\text{measured}}$

and we actuate the four magnets to create a droplet velocity that is along this displacement vector $\vec{v} = K\vec{d}$ (the scalar K is our control gain) so that the droplet moves towards its target location. The task of the control algorithm is to decide how to best actuate the four magnets to achieve the needed velocity.

The momentum of the ferrofluid is negligible. This means the droplet's has no ability to continue to travel if there is no applied force and it reacts immediately to any newly applied force. Thus the droplet's velocity is always in the direction of the magnetic force that we apply (this further means the droplet can execute sharp turns as we show in the results section). The task of the controller to create the needed droplet velocity can be phrased as creating a magnetic force in the right direction at the droplet's current location: the two only differ by a constant c , i.e. $\vec{v} = c\vec{F}_{mag}$. Although the droplet has no momentum, the electromagnets do. Their actuation cannot be changed sharply (due to coil charging time-constants) and our control takes this into account and compensates for it.

At each moment in time the control has to achieve a desired droplet velocity. This requirement sets two degrees of freedom: the velocity has an x and a y component. But there are four magnets. Thus we have two additional degrees of freedom left over for minimizing control effort. To do this, our control algorithm solves the following problem: it always restricts the four magnet actuations in such a way so as to exactly achieve the required velocity vector, it then further optimizes over the remaining two degrees of freedom to choose an actuation that minimizes the consumption of electrical power by the magnets.

The task of achieving a desired droplet velocity $\vec{v} = (v_x, v_y)$ can be phrased mathematically in terms of the set of algebraic quadratic equations:

$$\begin{aligned} k' \vec{u}^T [P_x(x,y)] \vec{u} &= v_x, \\ k' \vec{u}^T [P_y(x,y)] \vec{u} &= v_y. \end{aligned} \quad (12)$$

Now, minimizing the electrical power of the magnets is equivalent to minimizing the quadratic cost function:

$$J = \|\vec{u}\|^2 = \vec{u}^T \vec{u}. \quad (13)$$

Therefore, the control problem can be formulated in terms of minimizing (13), subject to the quadratic control constraints (12). Our approach to this optimization problem is to first identify a parametric family of all solutions of (12) (the constraint space), then explicitly express the cost function (13) in terms of the parameters of this family, and finally minimize the cost with respect to the parameters. This converts the original constrained optimization problem to an unconstrained problem. We outline these two steps below and refer to [84] for details.

At any specific (x,y) droplet location, for each desired velocity $\vec{v} = (v_x, v_y)$, the constraint space is a two-dimensional surface in the four-dimensional space of all possible actuations of the magnets—all points \vec{u} on this surface create the desired droplet velocity \vec{v} . Define the vector \vec{p} to be the magnetic field at the (x,y) location of the droplet

$$\sum_{j=1}^4 u_j \vec{H}_j(x,y) = \vec{p}. \quad (14)$$

Then the 2-dimensional quadratic constraint of Eq. (12) can be broken up into two equivalent linear constraints given by Eq. (14) and the next equation

$$2k' \sum_{j=1}^4 u_j \nabla(\vec{p}^T \vec{H}_j(x,y)) = \vec{v}. \quad (15)$$

We note that Eqs. (14) and (15) represent a set of two linear 2-dimensional equations (4 equations total) for \vec{u} and \vec{p} (for 6 unknowns) instead of one quadratic 2-dimensional equation for \vec{u} alone (2 equations for 4 unknowns). The advantage of the second formulation is that it is linear in \vec{u} (u_j appears only once in Eqs. (14) and (15), \vec{u} appears twice in each equation in (12)). If we choose a specific magnetic field direction, i.e. if we choose a \vec{p} , then we are left with 4 equations for the 4 actuation variables (u_1, u_2, u_3, u_4) . For any \vec{p} , we can easily solve for \vec{u} in terms of \vec{p} by a linear inversion. The end result is that the magnetic field itself, at the droplet's location, now parameterizes the choice of all possible magnet actuation currents via

$$\begin{aligned} \vec{u} &= \begin{bmatrix} \vec{H}_1(x,y) & \vec{H}_2(x,y) & \vec{H}_3(x,y) & \vec{H}_4(x,y) \\ \nabla(\vec{p}^T \vec{H}_1(x,y)) & \nabla(\vec{p}^T \vec{H}_2(x,y)) & \nabla(\vec{p}^T \vec{H}_3(x,y)) & \nabla(\vec{p}^T \vec{H}_4(x,y)) \end{bmatrix}^{-1} \\ &\times \begin{bmatrix} \vec{p} \\ \vec{v}/2k' \end{bmatrix} = \vec{g}(\vec{p}) \end{aligned} \quad (16)$$

that will achieve the desired droplet velocity \vec{v} . Now we have exactly satisfied the velocity constraint and can search simply over the magnetic field direction \vec{p} to find the minimum power control. (Remember that the magnetic field direction \vec{p} is *not* the direction of the applied magnetic force \vec{F}_{mag} or, equivalently, the created droplet velocity \vec{v} . The magnetic force is given by Eq. (4) and must be in the direction of the desired droplet velocity, the magnetic field is the remaining free parameter over which we now search to find the minimum electrical power control \vec{u}^* . This split of the problem into a force and field portion is both physically satisfying and yields a well conditioned optimization problem that can be solved cleanly.)

Now, the electrical power cost function $J = \vec{u}^T \vec{u} = \vec{g}^T(\vec{p}) \vec{g}(\vec{p})$ must be minimized over \vec{p} . This optimization problem is easier to solve using polar coordinates $\vec{p} = \rho \begin{bmatrix} \cos \phi & \sin \phi \end{bmatrix}$ for the magnetic field direction. We perform the optimization in two steps: we first minimize J with respect to ρ with ϕ fixed and we then minimize with respect to ϕ . The explicit form of $\vec{u} = \vec{g}(\vec{p})$ written in Eq. (16) allows for a closed form solution for the first step, while the second step requires a numerical optimization algorithm. This gives the final optimal control \vec{u}^* .

The nature of our resulting optimal control algorithm is illustrated in Figs. 3 and 4. It minimizes the amount of control effort used and explicitly accounts for the nonlinear nature of the magnetic force. The parameters used for generating these graphs are those of our experimental test-bed. Fig. 3 is for a simple case, where we wish to move a magnetic droplet along the x -axis from left to right with velocity $\vec{v} = (1,0)$. It shows the magnetic potential energy $U = -\|\vec{H}\|^2$ created in the petri dish as the drop moves through its $x = -0.7, -0.2, +0.2$ and $+0.7$ locations along the horizontal axis ($y=0$) with unit speed. The magnetic actuations (electrical currents) of each of the four magnets are also displayed (the sign denotes the polarity of the current, positive is clockwise). Notice how the actuation switches from the top and bottom magnets to mainly the right magnet as the droplet is moved from left to right. This is because when the droplet is far away from the right magnet it can be actuated to the right with lower current by using the closer top and bottom magnets.

Fig. 3 is for a droplet velocity that is always to the right. Fig. 4 shows how the 4 magnets must be actuated to control the ferrofluid droplet in any desired direction at any location in the petri dish. Each panel is for a different velocity direction (as shown by the small red line in the green circle at the top left of each panel). Inside each panel, for each droplet (x,y) location, the length of each of the four small lines is proportional to the electrical current that should be applied at each of the four

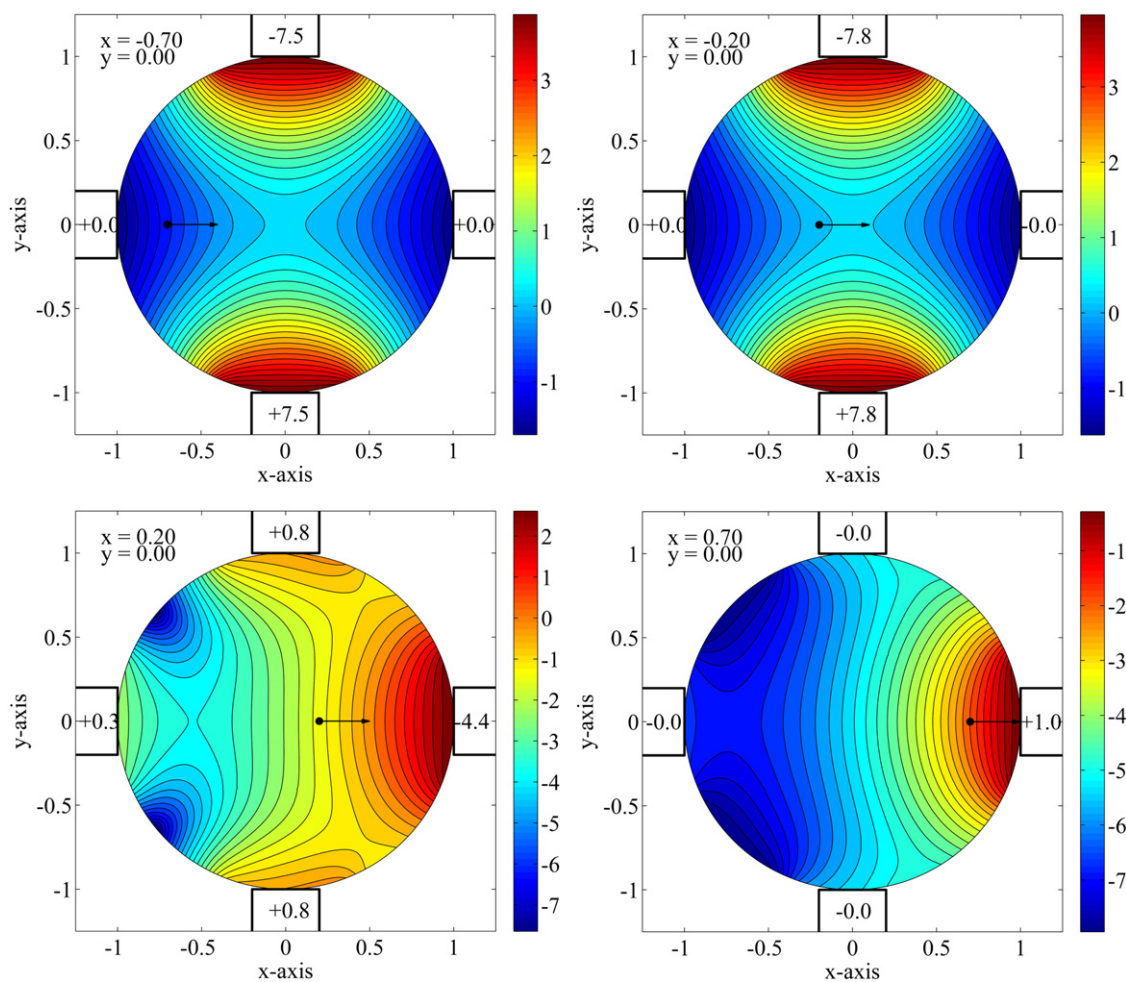


Fig. 3. Magnetic energy and magnet actuation for control of a ferrofluid droplet from left to right. Each panel is for a different (x,y) droplet location (the black dot). The black arrow is the direction of the desired (and thus applied) magnetic force, the color is the magnetic potential, which is equal to minus the magnetic field intensity squared (on a logarithmic scale), and the text inside each magnet states the current through that magnet (positive for clockwise current, negative for counter-clockwise).

magnets to move a droplet at that (x,y) location along the indicated velocity \vec{v} using minimum electrical power. The sign of the currents is coded with blue for positive and red for negative. This plot is read as follows: pick the panel that corresponds to the velocity direction that is desired, pick the current location of the ferrofluid drop in the petri dish, the 4 little lines at that location show what magnet currents should be applied in each of the 4 magnets (length corresponds to current strength, blue and red represent a negative or positive current) to move the droplet in the desired direction with minimum electrical power.

Fig. 4 determines the vector \vec{u} of the electrical currents to be applied to the magnets. However, as stated previously, we can only control the vector \vec{V} of the voltages of the magnets. The physical relationship between magnet currents \vec{u} and voltages \vec{V} is governed by the vector differential Eq. (9), a first order low-pass filter. It suppresses the high frequency temporal contents of the input \vec{V} and is characterized by its cut-off frequency $\omega = R/L$. To prevent distorting the desired value of \vec{u} , we compensate for the low-pass nature of the magnet physics by a linear high-pass filter in the control loop. This high-pass filter is designed in such a manner that its cascade combination with the low-pass magnet physics leads to a flat frequency response. We use the simplest high-pass filter for achieving this goal, which has a first order

structure with a zero exactly at ω (to cancel the pole of the low-pass filter) and a pole at $\omega' > \omega$, where ω' is the bandwidth of the output of the control algorithm.

The control also includes a second nonlinear filter. As the droplet moves through space, there are jumps in the type of control that is optimal. This is evident even from the simple straight-line motion case of Fig. 3, where it is first optimal to use the nearer top and bottom magnets (first 2 panels) until the droplet gets close enough to the right magnet so that its use becomes preferable (last panel). This kind of magnet switching is fundamental and, if there was no magnet charging time delays, the optimal control of Fig. 4 would attempt to apply discontinuous currents in time as the droplet moved through space. The magnet lag and linear high pass filter would smooth these out somewhat. Additionally, we have implemented a specially designed nonlinear filter that smoothes the jumps in time but still ensures that the direction of the applied current vector $\vec{u}(t) = [u_1(t) \ u_2(t) \ u_3(t) \ u_4(t)]^T$ accurately tracks the direction of the desired optimal current vector shown in Fig. 4 (mathematical filter details can be found in [84]). Since, as before, it is the direction of the control vector that sets the direction of the ferrofluid droplet motion, which in turn enables accurate correction of droplet position errors, this nonlinear filter enables a smooth control that does not degrade droplet manipulation performance.

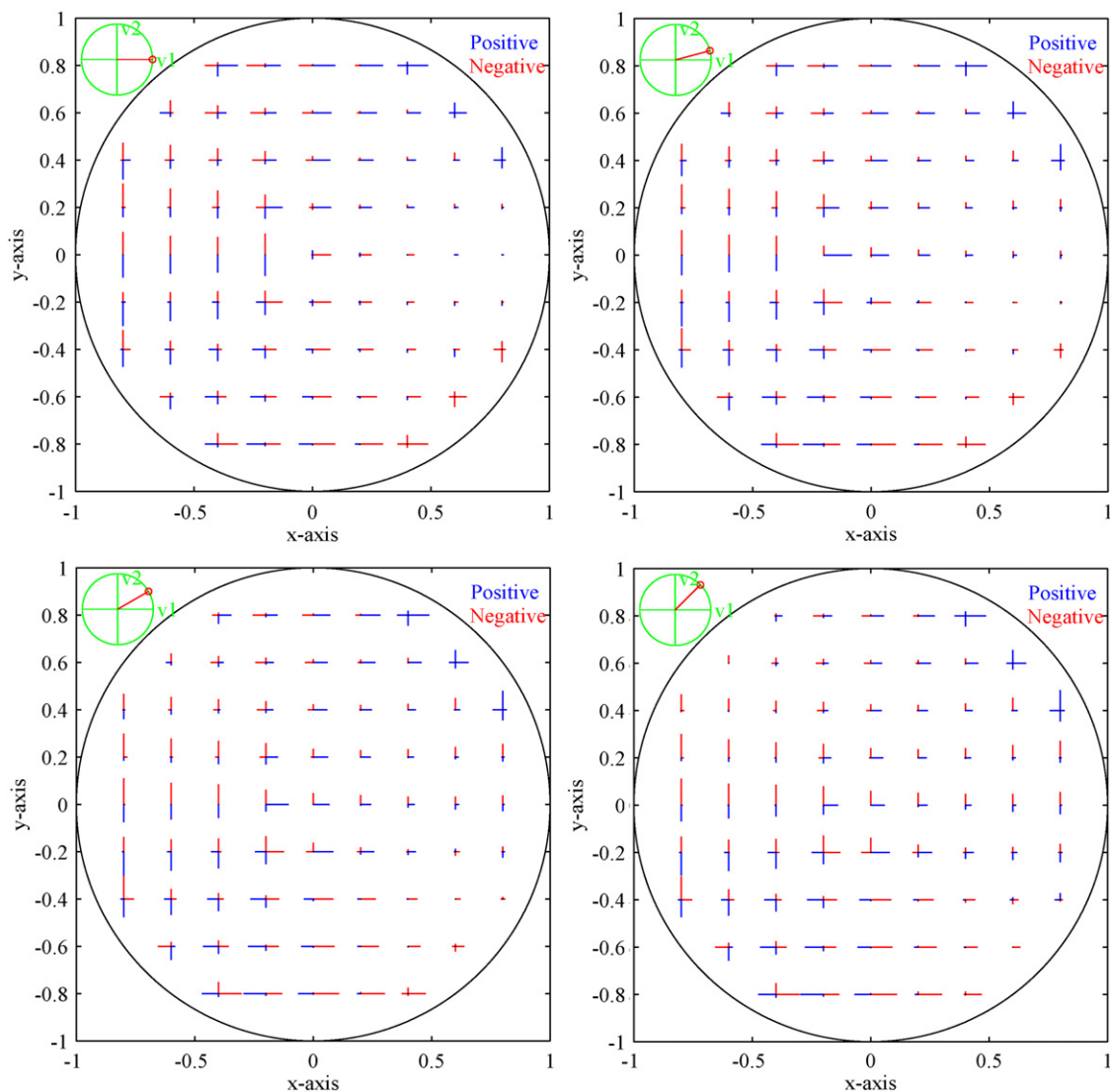


Fig. 4. Elements of the optimal control vector \underline{u} at different ferrofluid locations in the control region to attain the velocity direction shown at the top left of each panel with minimum electrical power. At each location, the length of each of the lines is proportional to the current to be applied to that magnet, the color (blue or red) corresponds to the sign of the current to be used. Four different directions for the desired velocity \underline{v} are shown: 0° , 15° , 30° and 45° with respect to the x -axis. Magnet actuations for the other seven 45° velocity direction sectors (each sector is half a quadrant) are symmetric 90° rotations and flips of the 4 cases shown. (For interpretation of the references to color in this figure legend, the reader is referred to the web version of this article.)

4. Experiment

In this section, we describe the details of the experimental setup. As shown in Fig. 1, there are four major components, the materials (petri dish, ferrofluid, liquid medium), the camera, the control algorithm software and hardware, and the electromagnets.

4.1. Materials used

We used a commercially available ferrofluid (Chemicell). The ferrofluid contains 8% by volume of 100 nm diameter multi-core particles. Each particle contains a 70–75 nm diameter starch encapsulated magnetite core that consists of a fused cluster of single-domain crystals. These magnetic particles were chosen for their size and high magnetic susceptibility ($\chi \sim 72$), which allowed them to be actuated at up to 4 cm away from our moderate strength electromagnets. A future experimental platform with strong magnets is currently under construction and will be able to manipulate a ferrofluid at a greater distance from the magnets.

A 1.5 inch. (3.8 cm) diameter petri dish (Fisher Scientific) was used to contain the ferrofluid. The petri dish was filled with a high viscosity mineral oil (Heavy Viscosity Mineral Oil, CQ Concepts), which served as a suspending medium for the droplet (as done in [85]). We used mineral oil because of its density, viscosity and surface tension properties, which caused the ferrofluid (which comes in the form of magnetic particles suspended in DI water) to remain as a single droplet and significantly reduces sticking of the ferrofluid to the petri dish surface.

4.2. Camera and real-time ferrofluid position detection software

The vision system consisted of a lens, camera, external lighting, and in-house imaging software. The camera (Guppy F-033B/C, 1st Vision) operated at 58 frames/s, had 656 by 494 color pixels, and was equipped with a 6 mm lens (1st Vision Inc.). A 56-LEDs ring light (Microscope Ring Light, AmScope) was mounted above the petri dish, around the camera, to create a shadow-free illumination of the ferrofluid.

The image software was coded in MATLAB version 2007b, with a Data Acquisition Toolbox (version 2.11) and an Image Acquisition Toolbox (version 3.0), and an Image Processing Toolbox (version 6.0), and ran on a Dell computer (2.4 GHz Intel Core2 Duo CPU). It allowed accurate real-time tracking and velocity estimation of the ferrofluid droplet or blob. This was achieved by combining an algorithm that finds all blobs in an image frame and an algorithm that tracks a blob of interest among other visual features. (It is possible for us to track one droplet through a field of many others [10] by using a Kalman tracking filter but this is not necessary for the results presented in this paper.) Each image frame is transferred from the camera to MATLAB through a firewire (IEEE 1394) interface. The image is thresholded, filtered, and operated on by an algorithm that finds the center of the ferrofluid droplet. This method finds and tracks the position of the ferrofluid droplet in less than 20 ms and passes that position to the control algorithm. The vision tracking is completely automated and does not require any user input during control operation.

4.3. Control algorithm implementation hardware and software

Like the vision code, the control algorithm is written in MATLAB and runs on the same computer as the droplet image tracking. It finds the optimal control magnet voltage actuation at each time by solving the mathematics described above, and it takes 66.7 ms to do so (hence the feedback loop runs at 15 Hz). This rate can be improved (e.g., by using C or MEX files to do the evaluation) and that will allow faster control of the ferrofluid in the future.

Output from the computer is used to command the four electromagnets. The computer is connected to a digital-to-analog signal converter (DAQ USB-3101, Measurement Computing), which connects to four linear DC servo amplifiers (MSE421, McLennan). The latter allows us to increase the low current, low voltage control signal (0–20 mA, ± 10 V) generated by the digital-to-analog signal converter to the higher current, higher voltage (0–1 A, ± 28 V) output signal required to power the four electromagnets.

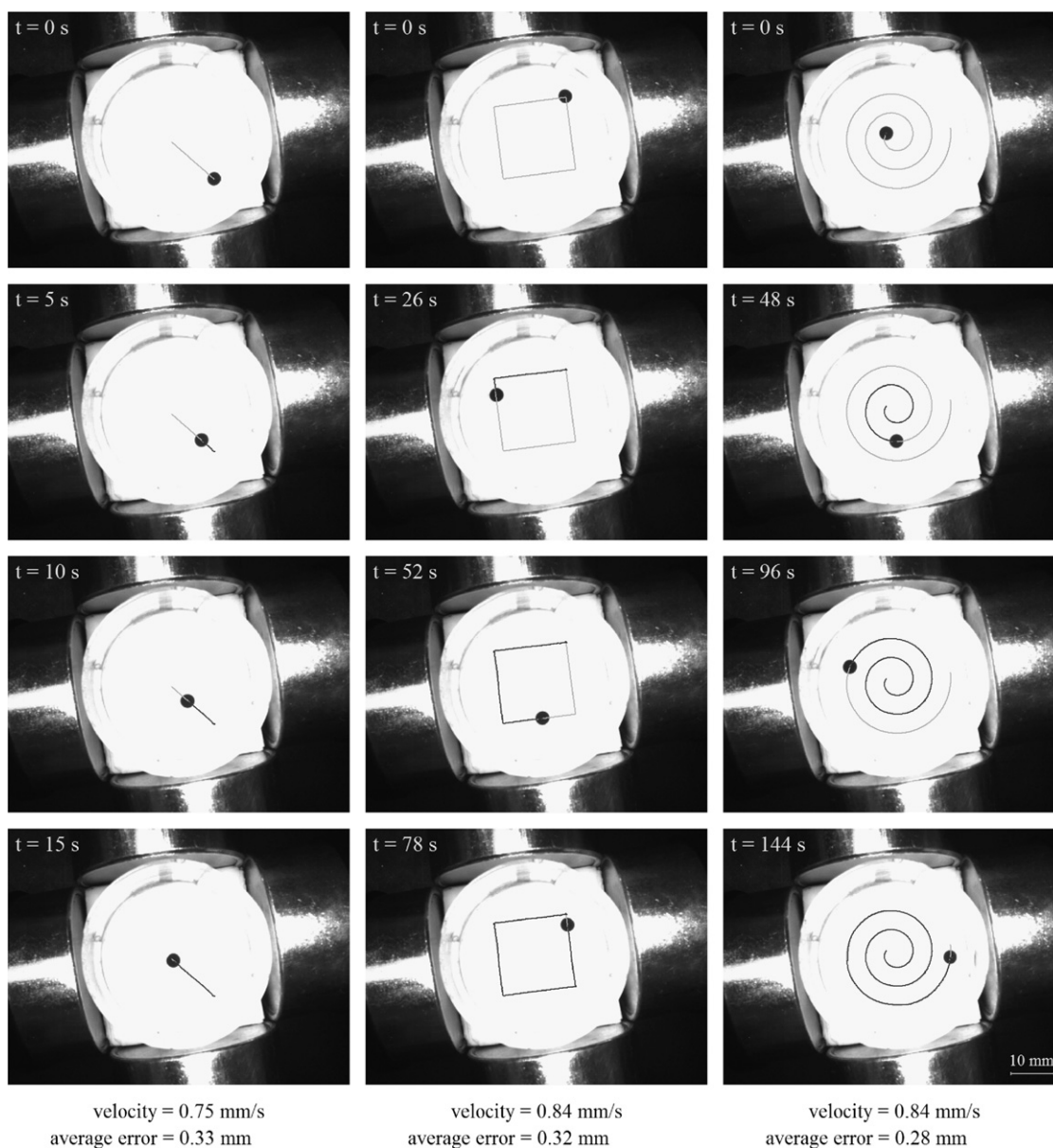


Fig. 5. Control of a medium size 20 μ L (1.7 mm radius) ferrofluid droplet slowly along a line, square, and spiral path. A quantitative measure of the average error (Eq. (17)) is noted at the bottom of each column.

4.4. Electromagnets

We used four small, inexpensive, and commercially available electromagnets to achieve the ferrofluid control results in this paper. These electromagnets (E-28-150 Tubular Electromagnet, Solenoidcity, \$57.51 each) have a length of 71.4 mm and a diameter of 38.1 mm each. They contain a 14 mm diameter iron core, their internal resistance was measured to be 43Ω , and they operate at 28 V while drawing 0.651 A. The strength of the magnets was unrated by the manufacturer but we measured the magnetic field distribution around these magnets with a 4.3 mm wide Hall probe (DC Magnetometer (Gauss), AlphaLab Inc.) on a square grid in the petri dish (with a placement accuracy of ~ 1 mm) and a field measurement accuracy of $\pm 2\%$ (as rated by the manufacturer) and verified that it matched the simulation data shown in Fig. 2. We found that these magnets generated a magnetic field of approximately 0.13 T at their faces, 0.20 T at their corners, and ~ 0.003 T at a distance of 3.7 cm, thus yielding a magnetic field of approximately ~ 0.016 T at the center of the petri dish.

During longer experimental runs, the magnets were cooled by rigid foam ice packs (Fisher Scientific) that were packed around them.

5. Results

We tested our magnetic control for a variety of ferrofluid droplet sizes and desired trajectory shapes and speeds. Droplet volumes were varied from 1 to 20 μL , which, under the action of surface tension, correspond to droplet radii of 0.6 and 1.7 mm, respectively. We also attempted control of a 150 μL droplet (3.3 mm radius) but this droplet was too large to be held together by surface tension during control and it broke apart. Trajectories were varied from the simplest to more complicated. The simplest task was to control the droplet in a straight line from its current to a desired location (to the center and to the outside of the petri dish). We also controlled the droplets in a square and spiral trajectory, and along 'UMD' lettering path (for the University of Maryland). Control speeds were varied from 0.033 to 0.11 mm/s.

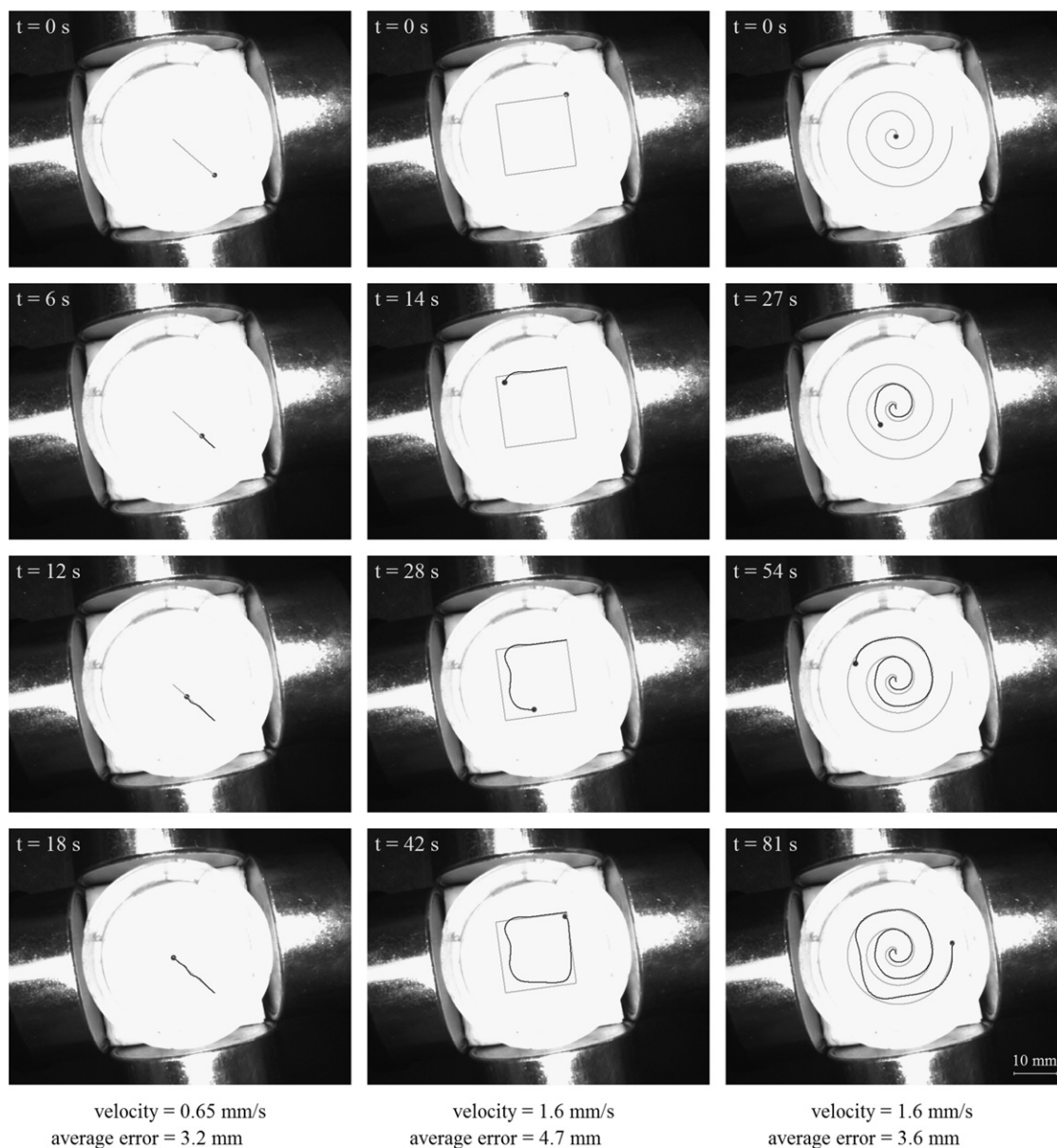


Fig. 6. Control of a small 1 μL (0.6 mm radius) ferrofluid droplet faster along a line, square, and spiral path.

Experimental results are shown in Figs. 5–8 and in additional figures in the supplementary material (doi:10.1016/j.jmmm.2010.08.024). In each figure the columns from left to right illustrate a straight line, square, and spiral trajectory. Time progresses from top to bottom and each snapshot shows a trace of the droplets motion for all preceding times. The average error between the desired and actual position of the ferrofluid droplet is defined as

$$e_{\text{path}} = \frac{1}{T} \int_0^T \|\vec{x}_{\text{desired}}(t) - \vec{x}_{\text{measured}}(t)\| dt, \quad (17)$$

where T is the amount of time it took to traverse the entire path. For each trajectory the average velocity and this quantitative average path error are noted on the bottom of that column. Below we show the easiest (medium droplet, slow motion) and hardest (small droplet, fast motion) two successful cases, as well as a third case that failed—the large droplet that broke up immediately under the applied magnetic actuation. We also show control along a more complicated ‘UMD’ path. The supplementary material provides figures for all the other cases tested (small droplet slow motion; medium droplet fast motion), as well as movies of the droplet behavior for all cases.

For control of the small 1 μL drop (Fig.6), the visible deviation of the ferrofluid from the desired square and spiral paths near the leftmost electromagnet contributes to most of the average positioning error. This deviation occurs in an operating regime where the magnets are being actuated near saturation. It is possible that the asymmetry seen in the path is due to the slightly different saturation characteristics between the four magnets, an aspect that has not yet been accounted for in the control design. Controlling the smaller droplet is harder. The medium size 20 μL droplet can be actuated with less force the magnets do not have to work as hard, and do not approach saturation; thus there is virtually no deviation even during fast control (see Figure SM-2 in the supplementary material (doi:10.1016/j.jmmm.2010.08.024)).

Beyond a certain ferrofluid droplet size, the current magnetic position control is no longer possible. For a 150 μL droplet

(see Fig. 7), applied magnetic forces exceed the surface tension forces that hold the droplet together and the droplet is broken up into sub-droplets. To close this results section we demonstrate control of a single ferrofluid droplet along a ‘UMD’ path, for the University of Maryland (Fig. 8).

Above we have shown optimal control of a single droplet to 4 cm depth using four medium-strength (0.13 T at their face), small, commercially available and inexpensive magnets. Based on our mathematical analysis above, using scaled-up stronger (2 T), larger (30 cm length, 30 cm coil diameter, 12 cm core diameter) electromagnets, will enable the same control forces on a single drop of ferrofluid at a depth of half a meter. Advanced magnets with optimally matched materials and shaped coils and cores, as presented in [86–88], could enable even stronger and deeper magnetic control forces.

6. Conclusion

This paper is concerned with precisely manipulating a ferrofluid by external magnets at a distance, and it considers the simplest archetypical example problem: control of a single droplet of ferrofluid in the plane by 4 electromagnets. The control algorithm explicitly takes into account the nonlinear pull-only nature of the magnetic actuation, it is designed for both the quadratic dependence of the magnetic force on the actuated strength of each magnet and the sharp drop-off of force with distance from each magnet. Control algorithm design is split into two parts. In the first, the set of all magnetic actuations is found that will move the droplet from where it is towards where it should be. In the second, from this set, the minimal electrical energy actuation is chosen and is applied to the magnets at each time. This gives a robust ability to actuate a single ferrofluid droplet between the four magnets, to any location or along any desired path. Successful numerical optimization and experiments results have shown how to address key practical issues of

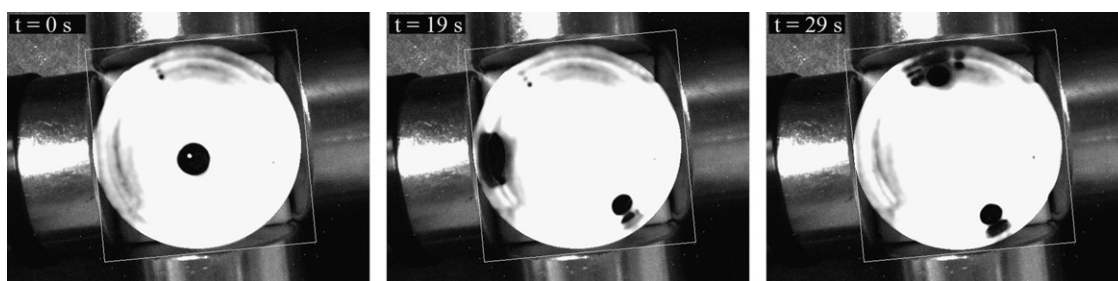


Fig. 7. Attempted control of a large 150 μL (3.3 mm radius) ferrofluid droplet. As soon as magnetic control is turned on, the droplet breaks up into multiple smaller droplets. This droplet was too big to control.



velocity = 1.6 mm/s
average error = 0.60 mm

Fig. 8. Control of a medium size 20 μL (1.7 mm radius) ferrofluid droplet slowly along a UMD path.

electromagnet charging time delays, magnet strength constraints, smooth switching between magnets, and the nonlinear dependence of the applied magnetic pull-only forces on space and electromagnetic currents.

Acknowledgements

This research was supported in part by NIBIB/NIH grant number R21EB009265. We thank Chemicell for supplying us with ferrofluid. We also thank Dr. Sedwick at the University of Maryland, USA, for providing help and advice on measurement of the magnetic fields and the resistive and inductance properties of the electromagnets.

Appendix A. Supporting materials

Supplementary data associated with this article can be found in the online version at doi:10.1016/j.jmmm.2010.08.024.

References

- [1] R.E. Rosensweig, *Ferrohydrodynamics*, Dover Publications, Inc., Mineola, NY, 1985.
- [2] C.I. Mikkelsen, *Magnetic Separation and Hydrodynamic Interactions in Microfluidic Systems*, in Department of Micro and Nanotechnology, Technical University of Denmark, Lyngby, Denmark, 2005.
- [3] R. Engel-Herbert, T. Hesjedal, Calculation of the magnetic stray field of a uniaxial magnetic domain, *Journal of Applied Physics* 97 (7) (2005) 74504–74505.
- [4] B. Shapiro, et al., Control to concentrate drug-coated magnetic particles to deep-tissue tumors for targeted cancer chemotherapy, in: Proceedings of the 46th IEEE International Conference on Decision and Control, New Orleans, LA, 2007.
- [5] B. Shapiro, et al., Dynamic control of magnetic fields to focus drug-coated nano-particles to deep tissue tumors, in: Proceedings of the Seventh International Conference on the Scientific and Clinical Applications of Magnetic Carriers, Vancouver, British Columbia, 2008.
- [6] Z. Cummins, et al., Manipulating ferrofluid at a distance: magnets pushing and dynamic control, in: Proceedings of the Eighth International Conference on the Scientific and Clinical Applications of Magnetic Carriers, Rostok, Germany, 2010.
- [7] B. Shapiro, Towards dynamic control of magnetic fields to focus magnetic carriers to targets deep inside the body, *Journal of Magnetism and Magnetic Materials* 321 (10) (2009) 1594–1599.
- [8] M. Armani, et al., Using feedback control and micro-fluidics to steer individual particles, in: Proceedings of the 18th IEEE International Conference on Micro Electro Mechanical Systems, Miami, FL, USA, 2005.
- [9] M. Armani, et al., Micro Flow Control Particle Tweezers in uTAS, Malmo, Sweden, 2004.
- [10] M. Armani, et al., Using feedback control and micro-fluidics to independently steer multiple particles, *Journal of Micro-Electro-Mechanical Systems* 15 (4) (2006) 945–956.
- [11] R.F. Probst, *Physicochemical Hydrodynamics: An Introduction*, 2 ed., John Wiley and Sons, Inc., New York, 1994.
- [12] P.C. Hiemenz, R. Rajagopalan, *Principles of Colloid and Surface Chemistry*, 3rd ed., Marcel Dekker, Inc., New York, Basel, Hong Kong, 1997.
- [13] U. Schillinger, et al., Advances in magnetofection—magnetically guided nucleic acid delivery, *Journal of Magnetism and Magnetic Materials* 293 (1) (2005) 501–508.
- [14] F.J. Alenghat, et al., Analysis of cell mechanics in single vinculin-deficient cells using a magnetic tweezer, *Biochemical and Biophysical Research Communications* 277 (1) (2000) 93–99.
- [15] B.G. Hosu, et al., Magnetic tweezers for intracellular applications, *Review of Scientific Instruments* 74 (9) (2003) 4158–4163.
- [16] A.H.B.d. Vries, et al., Micro magnetic tweezers for nanomanipulation inside live cells, *Biophysical Journal* 88 (3) (2005) 2137–2144.
- [17] J.S. Kanger, V. Subramaniam, R. van Driel, Intracellular manipulation of chromatin using magnetic nanoparticles, *Chromosome Research: An International Journal on the Molecular, Supramolecular and Evolutionary Aspects of Chromosome Biology* 16 (3) (2008) 511–522.
- [18] M.A.M. Gijjs, F.D.R. Lacharme, U. Lehmann, Microfluidic applications of magnetic particles for biological analysis and catalysis, *Chemical Reviews* 110 (3) (2009) 1518–1563.
- [19] U. Lehmann, et al., Two-dimensional magnetic manipulation of microdroplets on a chip as a platform for bioanalytical applications, *Sensors and Actuators B: Chemical* 117 (2) (2006) 457–463.
- [20] A.S. Lubbe, et al., Clinical experiences with magnetic drug targeting: a phase I study with 4'-epidoxorubicin in 14 patients with advanced solid tumors, *Cancer Research* 56 (20) (1996) 4686–4693.
- [21] A.S. Lubbe, et al., Preclinical experiences with magnetic drug targeting: tolerance and efficacy, *Cancer Research* 56 (20) (1996) 4694–4701.
- [22] E.K. Ruuge, A.N. Rusetski, Magnetic fluids as drug carriers—targeted transport of drugs by a magnetic-field, *Journal of Magnetism and Magnetic Materials* 122 (1–3) (1993) 335–339.
- [23] A.S. Lubbe, et al., Physiological aspects in magnetic drug-targeting, *Journal of Magnetism and Magnetic Materials* 194 (1–3) (1999) 149–155.
- [24] A.S. Lubbe, C. Alexiou, C. Bergemann, Clinical applications of magnetic drug targeting, *Journal of Surgical Research* 95 (2) (2001) 200–206.
- [25] C. Alexiou, et al., Magnetic drug targeting—biodistribution of the magnetic carrier and the chemotherapeutic agent mitoxantrone after locoregional cancer treatment, *Journal of Drug Targeting* 11 (3) (2003) 139–149.
- [26] Z.G. Forbes, et al., An approach to targeted drug delivery based on uniform magnetic fields, *IEEE Transactions on Magnetics* 39 (5) (2003) 3372–3377.
- [27] A.J. Lemke, et al., MRI after magnetic drug targeting in patients with advanced solid malignant tumors, *European Radiology* 14 (11) (2004) 1949–1955.
- [28] C. Simon, Magnetic drug targeting. New paths for the local concentration of drugs for head and neck cancer, *HNO* 53 (7) (2005) 600–601.
- [29] C. Alexiou, et al., Distribution of mitoxantrone after magnetic drug targeting: fluorescence microscopic investigations on VX2 squamous cell carcinoma cells, *Zeitschrift Fur Physikalische Chemie—International Journal of Research in Physical Chemistry & Chemical Physics* 220 (2) (2006) 235–240.
- [30] P. Xiong, et al., Theoretical research of magnetic drug targeting guided by an outside magnetic field, *Acta Physica Sinica* 55 (8) (2006) 4383–4387.
- [31] B. Polyak, G. Friedman, Magnetic targeting for site-specific drug delivery: applications and clinical potential, *Expert Opinion on Drug Delivery* 6 (1) (2009) 53–70.
- [32] A. Beyzavi, N.-T. Nguyen, Programmable two-dimensional actuation of ferrofluid droplet using planar microcoils, *Journal of Micromechanics and Microengineering* 20(1)015018–015018.
- [33] Q. Ramadan, et al., Microcoils for transport of magnetic beads, *Applied Physics Letters* 88 (3) (2006) 032501–032503.
- [34] F. Amblard, et al., A magnetic manipulator for studying local rheology and micromechanical properties of biological systems, *Review of Scientific Instruments* 67 (3) (1996) 818–827.
- [35] C. Gosse, Magnetic tweezers: micromanipulation and force measurement at the molecular level, *Biophysical Journal* 82 (6) (2002) 3314–3329.
- [36] J.K. Fisher, et al., Thin-foil magnetic force system for high-numerical-aperture microscopy, *Review of Scientific Instruments* 77 (2) (2006) 023702–023702.
- [37] K.C. Neuman, A. Nagy, Single-molecule force spectroscopy: optical tweezers, magnetic tweezers and atomic force microscopy, *Nature Methods* 5 (6) (2008) 491–505.
- [38] H.A. Pohl, *Dielectrophoresis: The Behavior of Neutral Matter in Nonuniform Electric Fields*, Cambridge University Press, Cambridge, 1978.
- [39] B.H. Lapizco-Encinas, M. Rito-Palomares, Dielectrophoresis for the manipulation of nanobioparticles, *Electrophoresis* 28 (24) (2007) 4521–4538.
- [40] B. Edwards, N. Engheta, S. Evoy, Electric tweezers: experimental study of positive dielectrophoresis-based positioning and orientation of a nanorod, *Journal of Applied Physics* 102 (2007) 024913.
- [41] D.C. Meeker, et al., Optimal realization of arbitrary forces in a magnetic stereotaxis system, *IEEE Transactions on Magnetics* 32 (2) (1996) 320–328.
- [42] F.M. Creighton, Control of Magnetomotive Actuators for an Implanted Object in Brain and Phantom Materials, in Department of Physics, University of Virginia, Charlottesville, 1991, p. 203.
- [43] M.A. Howard III, R.C. Ritter, M.S. Grady, *Video Tumor Fighting System*, USA, 1989.
- [44] Y.M. Eyssa, Apparatus and methods for controlling movement of an object through a medium using a magnetic field–, 2005.
- [45] R.C. Ritter, Open field system for magnetic surgery, USA, 2001.
- [46] P.R. Werp, Methods and apparatus for magnetically controlling motion direction of a mechanically pushed catheter, 2002.
- [47] F.J. Bova, W.A. Friedman, *Computer Controlled Guidance of a Biopsy Needle*, University of Florida, US, 2003.
- [48] R.C. Ritter, P.R. Werp, M.A. Lawson, *Method and Apparatus for Rapidly Changing a Magnetic Field Produced by Electromagnets*, Stereotaxis, Inc. (St. Louis, MO): US, 2000.
- [49] S. Martel, et al., Automatic navigation of an untethered device in the artery of a living animal using a conventional clinical magnetic resonance imaging system, *Applied Physics Letters* 90 (4) (2007) 114105–114111.
- [50] J.-B. Mathieu, G. Beaudoin, S. Martel, Method of propulsion of a ferromagnetic core in the cardiovascular system through magnetic gradients generated by an MRI system, *IEEE Transactions on Biomedical Engineering* 53 (2) (2006) 292–299.
- [51] S. Tamaz, et al., Real-time MRI-based control of a ferromagnetic core for endovascular navigation, *IEEE Transactions on Biomedical Engineering* 55 (7) (2008) 1854–1863.
- [52] K.B. Yesin, K. Vollmers, B.J. Nelson, Modeling and control of untethered biomicrobots in a fluidic environment using electromagnetic fields, *The International Journal of Robotics Research* 25 (5–6) (2006) 527–536.
- [53] K.B. Yesin, K. Vollmers, B.J. Nelson, in: Proceedings of ICRA '04 IEEE International Conference on Analysis and Design of Wireless Magnetically Guided Microrobots in Body Fluids, in Robotics and Automation, 2004.

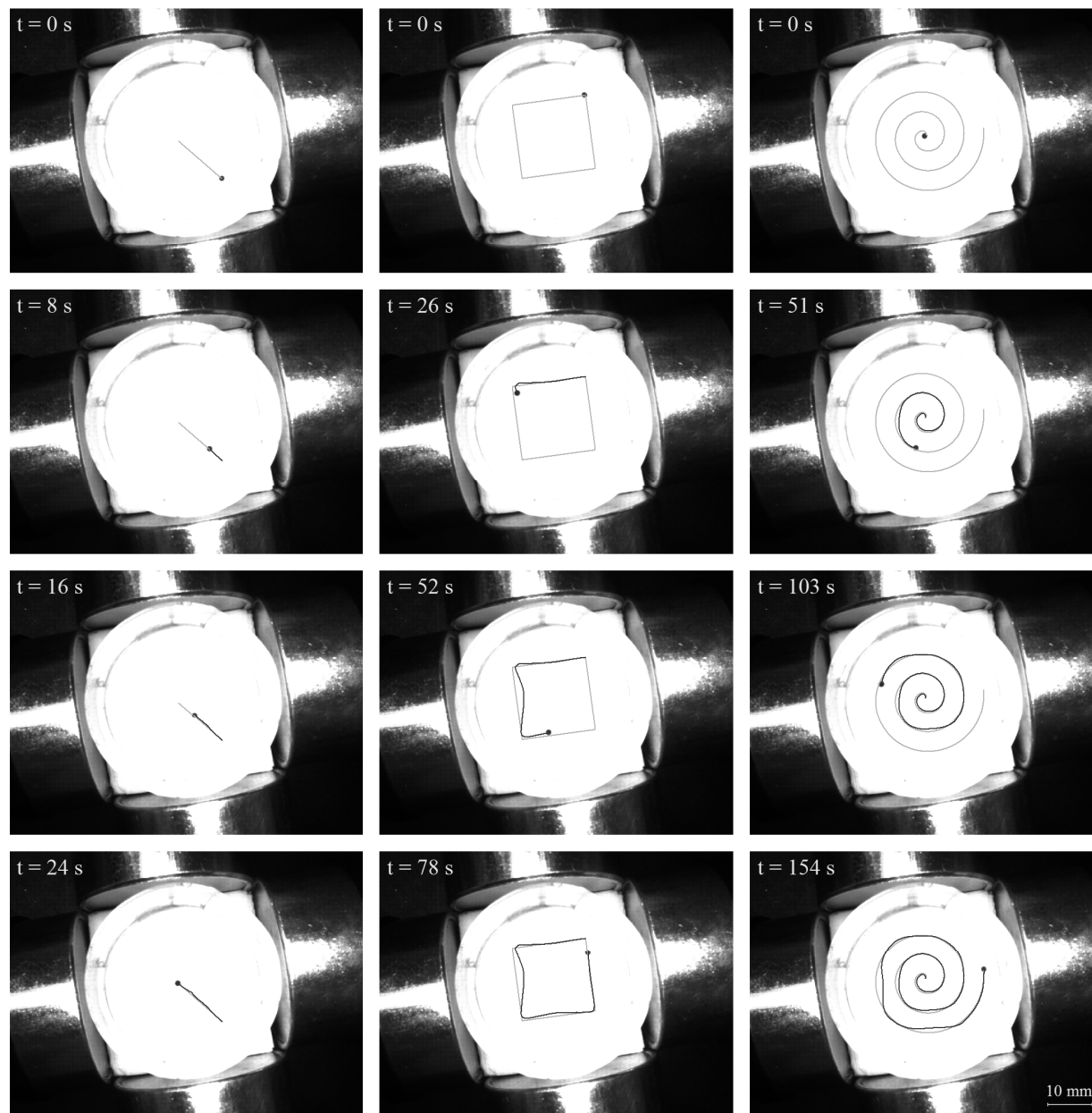
- [54] J.B. Mathieu, S. Martel, In vivo validation of a propulsion method for untethered medical microrobots using a clinical magnetic resonance imaging system, 2007.
- [55] S. Martel, et al., Flagellated magnetotactic bacteria as controlled MRI-trackable propulsion and steering systems for medical nanorobots operating in the human microvasculature, *The International Journal of Robotics Research* 28 (4) (2009) 571–582.
- [56] S. Martel, O. Felfoul, M. Mohammadi, in: 2nd IEEE RAS & EMBS International Conference on Flagellated Bacterial Nanorobots for Medical Interventions in the human body, in *Biomedical Robotics and Biomechatronics, BioRob 2008*, 2008.
- [57] H.E. Potts, R.K. Barrett, D.A. Diver, Dynamics of freely-suspended drops, *Journal of Physics D—Applied Physics* 34 (17) (2001) 2629–2636.
- [58] J. Lipfert, X. Hao, N.H. Dekker, Quantitative modeling and optimization of magnetic tweezers, *Biophysical Journal* 96 (12) (2009) 5040–5049.
- [59] M.W. Wilson, et al., Hepatocellular carcinoma: regional therapy with a magnetic targeted carrier bound to doxorubicin in a dual MR imaging/conventional angiography suite—initial experience with four patients, *Radiology* 230 (1) (2004) 287–293.
- [60] K.J. Widder, et al., Tumor remission in yoshida sarcoma-bearing rats by selective targeting of magnetic albumin microspheres containing doxorubicin, *Proceedings of National Academy Sciences* 78 (1) (1981) 579–581.
- [61] U.O. Hafeli, et al., Effective targeting of magnetic radioactive ⁹⁰Y-microspheres to tumor cells by an externally applied magnetic field. Preliminary in vitro and in vivo results, *Nuclear Medicine and Biology* 22 (2) (1995) 147–155.
- [62] S. Goodwin, et al., Targeting and retention of magnetic targeted carriers (MTCs) enhancing intra-arterial chemotherapy, *Journal of Magnetism and Magnetic Materials* 194 (1–3) (1999) 132–139.
- [63] S.C. Goodwin, et al., Single-dose toxicity study of hepatic intra-arterial infusion of doxorubicin coupled to a novel magnetically targeted drug carrier, *Toxicological Sciences* 60 (1) (2001) 177–183.
- [64] T. Kubo, et al., Targeted delivery of anticancer drugs with intravenously administered magnetic liposomes in osteosarcoma-bearing hamsters, *International Journal of Oncology* 17 (2) (2000) 309–315.
- [65] K. Hirao, et al., Targeted gene delivery to human osteosarcoma cells with magnetic cationic liposomes under a magnetic field, *International Journal of Oncology* 22 (5) (2003) 1065–1071.
- [66] J.A. Ritter, K.D. Daniel, A.D. Ebner, High gradient magnetic implants for targeted drug delivery, *Abstracts of Papers of the American Chemical Society*, vol. 225, 2003, pp. U991–U992.
- [67] G.H. Iacoba, et al., Magnetizable needles and wires—modeling an efficient way to target magnetic microspheres in vivo, *Biorheology* 41 (2004) 599–612.
- [68] M.O. Aviles, et al., Theoretical analysis of a transdermal ferromagnetic implant for retention of magnetic drug carrier particles, *Journal of Magnetism and Magnetic Materials* 293 (1) (2005) 605–615.
- [69] A.J. Rosengart, et al., Magnetizable implants and functionalized magnetic carriers: a novel approach for noninvasive yet targeted drug delivery, *Journal of Magnetism and Magnetic Materials* 293 (1) (2005) 633–638.
- [70] O. Rotariu, N.J.C. Strachan, Modeling magnetic carrier particle targeting in the tumor microvasculature for cancer treatment, *Journal of Magnetism and Magnetic Materials—Proceedings of the Fifth International Conference on Scientific and Clinical Applications of Magnetic Carriers* 293 (1) (2005) 639–646.
- [71] B.B. Yellen, et al., Targeted drug delivery to magnetic implants for therapeutic applications, *Journal of Magnetism and Magnetic Materials* 293 (1) (2005) 647–654.
- [72] R.P. Feynman, R.B. Leighton, M. Sands, *The Feynman Lectures on Physics*, Addison–Wesley Publishing Company, 1964.
- [73] D.A. Fleisch, *A Student's Guide to Maxwell's Equations*, Cambridge University Press, Cambridge, UK; New York, 2008.
- [74] Z.G. Forbes, et al., Validation of high gradient magnetic field based drug delivery to magnetizable implants under flow, *IEEE Transactions on Biomedical Engineering* 2 Part 1 (2008) 643–649.
- [75] F.P. Incropera, *Fundamentals of Heat and Mass Transfer*, John Wiley, Hoboken, NJ, 2007.
- [76] W.M. Saltzman, *Drug Delivery: Engineering Principles for Drug Therapy*, Oxford University Press, New York, NY, 2001.
- [77] N.P. Smith, A.J. Pullan, P.J. Hunter, An anatomically based model of transient coronary blood flow in the heart, *SIAM Journal on Applied Mathematics* (2001) 990–1018.
- [78] S. Odenbach, *Magnetoviscous Effects in Ferrofluids*, Springer, 2002.
- [79] A.Y. Zubarev, S. Odenbach, J. Fleischer, Rheological properties of dense ferrofluids. Effect of chain-like aggregates, *Journal of Magnetism and Magnetic Materials* 252 (2002) 241–243.
- [80] M. Wu, et al., Magnetic field-assisted hydrothermal growth of chain-like nanostructure of magnetite, *Chemical Physics Letters* 401 (4–6) (2005) 374–379.
- [81] V.S. Mendeleev, A.O. Ivanov, Ferrofluid aggregation in chains under the influence of a magnetic field, *Physical Review E* 70 (5) (2004) 51502.
- [82] Z. Wang, C. Holm, Structure and magnetic properties of polydisperse ferrofluids: a molecular dynamics study, *Physical Review E* 68 (4) (2003) 41401.
- [83] C.A. Desoer, E.S. Kuh, *Basic Circuit Theory: Chapters 1 Through 10*, McGraw-Hill Inc., US, 1969.
- [84] A. Komae, B. Shapiro, Steering a ferromagnetic particle by magnetic feedback control: algorithm design and validation, *American Control Conference (ACC)*, 30 June–2 July, 2010, pp. 6543–6548, URL: <http://ieeexplore.ieee.org/stamp/stamp.jsp?tp=&arnumber=5531414&isnumber=5530425>.
- [85] U. Lehmann, et al., Two-dimensional magnetic manipulation of microdroplets on a chip as a platform for bioanalytical applications, *Sensors and Actuators B: Chemical* 117 (2) (2005) 457–463.
- [86] F.M. Creighton, Optimal distribution of magnetic material for catheter and guidewire cardiology therapies. in: *Proceedings of the IEEE International Magnetism Conference, INTERMAG, 2006*, San Diego, CA, USA.
- [87] J.-S. Choi, J. Yoo, Design of a Halbach magnet array based on optimization techniques, *IEEE Transactions on Magnetics* 44 (10) (2008) 2361–2366.
- [88] C. Alexiou, et al., IEEE Transactions on a high field gradient magnet for magnetic drug targeting, *Applied Superconductivity* 16 (2) (2006) 1527–1530.

**Planar Steering of a Single Ferrofluid Drop by Optimal Minimum Power
Dynamic Feedback Control of Four Electromagnets at a Distance**

R. Probst, J. Lin, A. Komae, A. Nacev, Z. Cummins, B. Shapiro*
*Fischell Department of Bio-Engineering, 3178 Martin Hall,
University of Maryland, College Park, MD 20742. benshap@umd.edu

Supplementary Material

1. Additional Figures Experiment Results

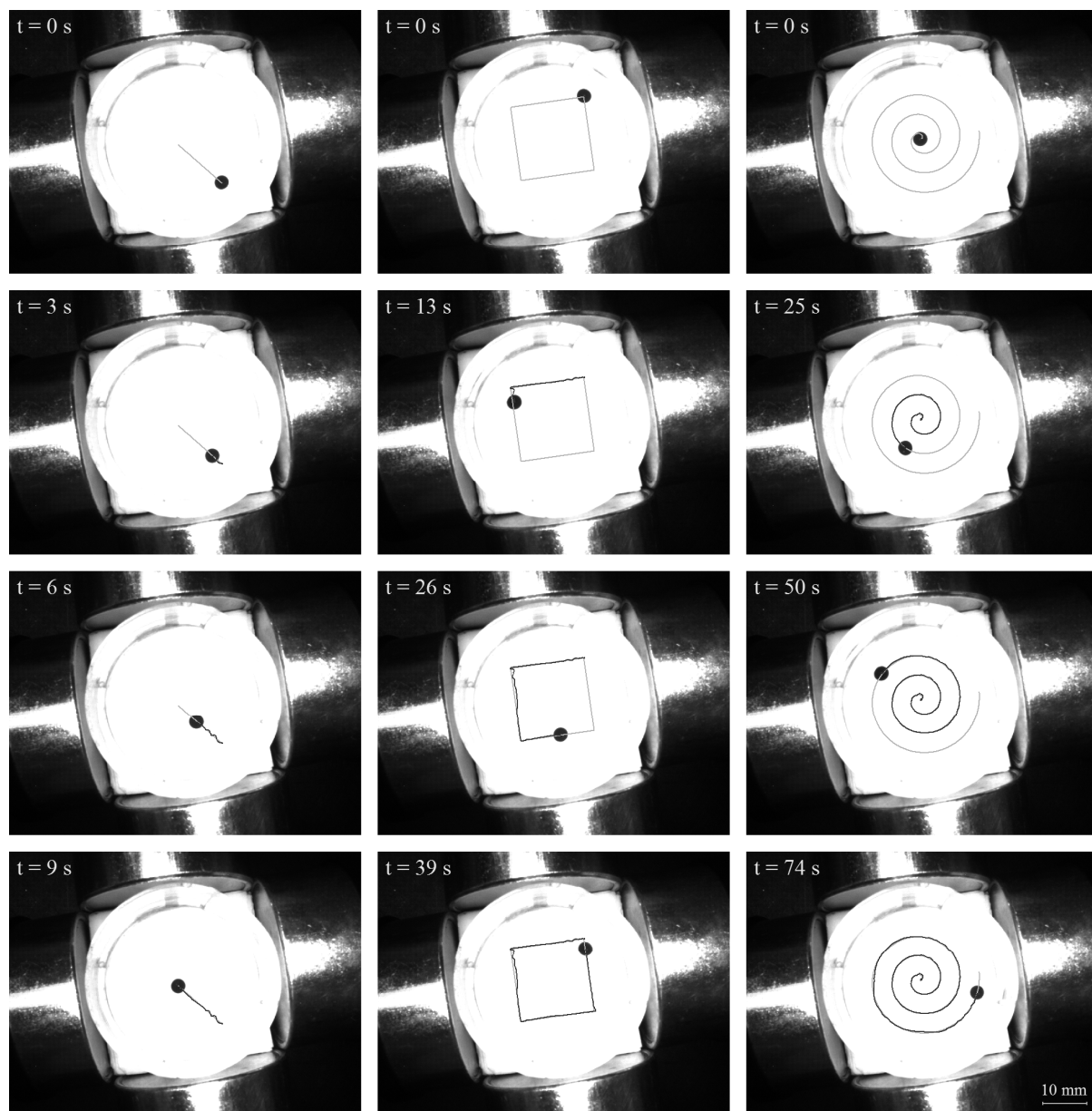


velocity = 0.50 mm/s
average error = 2.1 mm

velocity = 0.83 mm/s
average error = 2.3 mm

velocity = 0.81 mm/s
average error = 1.7 mm

Figure SM-1: Control of a small 1 μL (0.6 mm radius) ferrofluid droplet slowly along a line, square, and spiral path (desired path: gray line; actual path: black line). A quantitative measure of the average error (equation Error! Reference source not found.) is noted at the bottom of each column.



velocity = 1.1 mm/s
average error = 0.55 mm




velocity = 1.7 mm/s
average error = 0.63 mm

velocity = 1.6 mm/s
average error = 0.51 mm

Figure SM-2: Control of a medium size 20 μ L (1.7 mm radius) ferrofluid droplet faster along a line, square, and spiral path.

2. Movies of Experimental Results

Movie of Figure SM-1 (line)	 5a.mpg
Movie of Figure SM-1 (square)	 5b.mpg
Movie of Figure SM-1 (spiral)	 5c.mpg
Movie of Figure SM-2 (line)	 8a.mpg
Movie of Figure SM-2 (square)	 8b.mpg
Movie of Figure SM-2 (spiral)	 8c.mpg
Movie of Figure 5 (line)	 7a.mpg
Movie of Figure 5 (square)	 7b.mpg
Movie of Figure 5 (spiral)	 7c.mpg
Movie of Figure 6 (line)	 6a.mpg

Movie of Figure 6 (square)	 6b.mpg
Movie of Figure 6 (spiral)	 6c.mpg
Movie of Figure 8 (UMD)	 8.mpg

3. Appendix

3.1. Computing the Magnetic Field for a Single Electromagnet

Here we derive and compute the magnetic field around a single electromagnet (Figure 2). We consider an N -loop solenoid with a constant coil radius a (the thickness of the coil is ignored) and length l , and assume that a current I passes through the solenoid. The solenoid axis is along the z -axis of a coordinate system such that the solenoid is extended from $z = 0$ toward $z = -l$. We determine the magnetic field $\vec{B}(\vec{r})$ at any arbitrary point $\vec{r} = (x, y, z)$ with $z > 0$.

Let $\vec{B}_s(\vec{r})$ be the magnetic field due to a single loop of the solenoid in the xy plane. Then, by the linearity of Maxwell's equations, the total magnetic field can be expressed as

$$(A 1.1) \quad \vec{B}(\vec{r}) = \sum_{n=0}^{N-1} \vec{B}_s(x, y, z + (n/N)l),$$

which can be approximated by an integral formulation

$$(A 1.2) \quad \begin{aligned} \vec{B}(\vec{r}) &= \frac{N}{l} \sum_{n=0}^{N-1} \vec{B}_s(x, y, z + (n/N)l) \frac{l}{N} \\ &\approx \frac{N}{l} \int_0^l \vec{B}_s(x, y, z + u) du \\ &= N \int_0^l \vec{B}_s(x, y, z + lv) dv. \end{aligned}$$

We use the Biot-Savart law to determine the magnetic field due to a single loop. This law describes the magnetic field due to a differential element $d\vec{\ell}$ of a wire according to

$$(A 1.3) \quad d\vec{B}_s = \frac{\mu_0 I}{4\pi} \cdot \frac{d\vec{\ell} \times \vec{s}}{\|\vec{s}\|^3},$$

where μ_0 is the permeability of free-space, \vec{s} is the displacement vector from the wire differential element to the point at which the field is being computed, and $d\vec{B}_s$ is the differential contribution of $d\vec{\ell}$ to the total magnetic field. Let $\vec{q} = (a \cos \phi, a \sin \phi, 0)$ be the position vector of a point on the loop, where ϕ is the angle between \vec{q} and the x -axis. Then, $d\vec{\ell}$ and \vec{s} can be represented as $d\vec{\ell} = (-a \sin \phi, a \cos \phi, 0)$ and $\vec{s} = \vec{r} - \vec{q} = (x - a \cos \phi, y - a \sin \phi, z)$. Substituting these vectors into (A 1.3) and integrating over $\phi \in [0, 2\pi]$, we get

$$(A 1.4) \quad \vec{B}_s(\vec{r}) = \frac{\mu_0 I a}{4\pi} \int_0^{2\pi} \frac{d\phi}{\left((x - a \cos \phi)^2 + (y - a \sin \phi)^2 + z^2 \right)^{3/2}} \cdot (z \cos \phi, z \sin \phi, a - x \cos \phi - y \sin \phi).$$

Substituting this result into (A 1.2), we obtain the total magnetic field

$$(A 1.5) \quad \begin{aligned} \vec{B}(\vec{r}) &= \frac{\mu_0 N I a}{4\pi} \int_0^l \int_0^{2\pi} \frac{d\phi dv}{\left((x - a \cos \phi)^2 + (y - a \sin \phi)^2 + (z + lv)^2 \right)^{3/2}} \\ &\quad \times \left((z + lv) \cos \phi, (z + lv) \sin \phi, a - x \cos \phi - y \sin \phi \right). \end{aligned}$$

With some efforts, we can simplify this expression to

$$(A 1.6) \quad \vec{B}(\vec{r}) = \frac{\mu_0 N I}{4\pi a} \cdot \frac{1}{\theta} \cdot \begin{pmatrix} g_1(x/a, y/a, z/a) - g_1(x/a, y/a, z/a + \theta) \\ g_1(y/a, x/a, z/a) - g_1(y/a, x/a, z/a + \theta) \\ g_2(x/a, y/a, z/a) - g_2(x/a, y/a, z/a + \theta) \end{pmatrix}$$

where $\theta = l/a$ and g_1 and g_2 are defined as

$$(A 1.7) \quad g_1(\vec{r}) = \int_0^{2\pi} \frac{\cos \phi d\phi}{((x - \cos \phi)^2 + (y - \sin \phi)^2 + z^2)^{1/2}}$$

$$g_2(\vec{r}) = \int_0^{2\pi} \frac{z}{(x - \cos \phi)^2 + (y - \sin \phi)^2 + z^2} \cdot \frac{(x \cos \phi + y \sin \phi - 1) d\phi}{((x - \cos \phi)^2 + (y - \sin \phi)^2 + z^2)^{1/2}}.$$

For any droplet position \vec{r} , the above two integrals are easily computed numerically using the trapezoidal or Simpson's rule.

The magnet length ($l = 71.4$ mm) and inner coil radius ($a = 7$ mm) are stated in Section **Error! Reference source not found.**. However, we do not precisely know N , the number of loops, because we are treating these solid core magnets as air filled for mathematical simplicity and because the properties of the core are not stated by the manufacturer. As a result, N is our single free parameter and we choose it to best match our measured magnetic field data. Figure SM-3 shows a comparison between the predicted and experimentally measured x -component of the magnetic field for the magnet on the right of the petri dish.

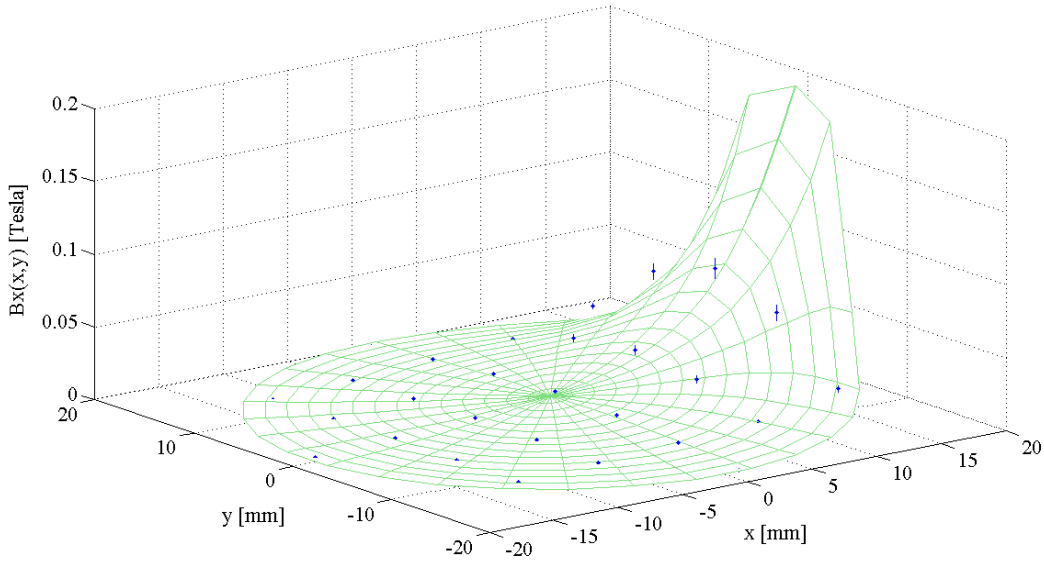


Figure SM-3: The predicted versus the measured magnetic field when the right-most magnet is turned on to its maximum value of 28 volts. The vertical axis shows the x -component of the magnetic field (B_x) for (x,y) locations in the petri-dish. The green mesh corresponds to the theory calculated above, the blue dots with the small vertical lines show the measured data and its error bars.

Using the values of a , l , I and N above and plotting the log of the magnetic field intensity squared gives the coloring of Figure 2. As can be seen both above and on the logarithm scale of Figure 2, the magnetic field strength drops rapidly with distance from the electromagnet.

3.2. Measurement of the Ferrofluid Droplet Magnetic Drift Coefficient k'

This section describes our measurements and methods to infer the value of the magnetic drift coefficient k' in equation **Error! Reference source not found.** for the ferrofluid droplet. The purpose here is to quantify the bulk behavior of the droplet, not to infer the detailed physics of magnetic particle-to-particle interactions (readers interested in that aspect can refer to, for example, [1-5]).

Two droplet volumes (5 and 7.5 μL) were placed near the center of the control domain and a single magnet was turned on to pull the droplet towards it. Time and position data of the droplet was recorded and compared to the motion predicted by our theoretical model (equations **Error! Reference source not found.**-**Error! Reference source not found.**, Figure 2, and equation **Error! Reference source not found.**) for a range of k' values. Figure SM-4 shows a comparison of the measured droplet movement (blue circles with error bars) to the predicted motion assuming the constant k' coefficient shown for each green curve.

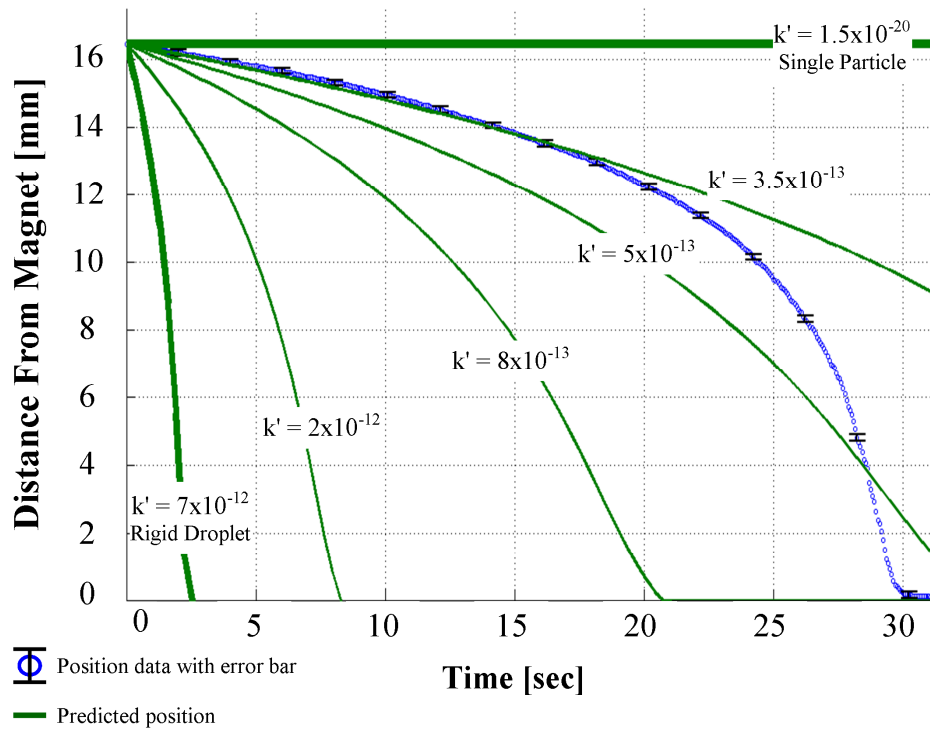


Figure SM-4: Time and position data of a 5 μL droplet (blue circles with error bars) compared with predictions from the model (green lines). Motions for various constant k' coefficients are plotted ranging from the k' value for a single nano-particle to a k' value for the whole droplet treated as one rigid ferromagnetic bead. The two nearest curves to the experimentally measured positions have an average error of $(|X_{\text{theory}} - X_{\text{experiment}}|/|X_{\text{experiment}}|) = 4\%$ and 33% up until 20 seconds for $k' = 3.5 \times 10^{-13}$ and $k' = 5 \times 10^{-13}$ respectively.

From this figure, it is clear that there is a best-fit k' value ($3.5 \times 10^{-13} \text{ m}^4/\text{A}^2 \text{ s}$ for this case) and it is also clear that a constant k' value does not adequately predict the fast snap-to-the-magnet droplet motion at the end of the trajectory (for $t > 20$ seconds). To quantify the change in k' over time we used the definition of k' stated in equation **Error! Reference source not found.** We plotted the droplets instantaneous drift velocity versus the gradient of the magnetic field squared at each location and divided one by the other to give us a measure of k' at each instant in time. From this we then further plotted the instantaneous k' against the magnetic field strength at that time and location (Figure SM-6).

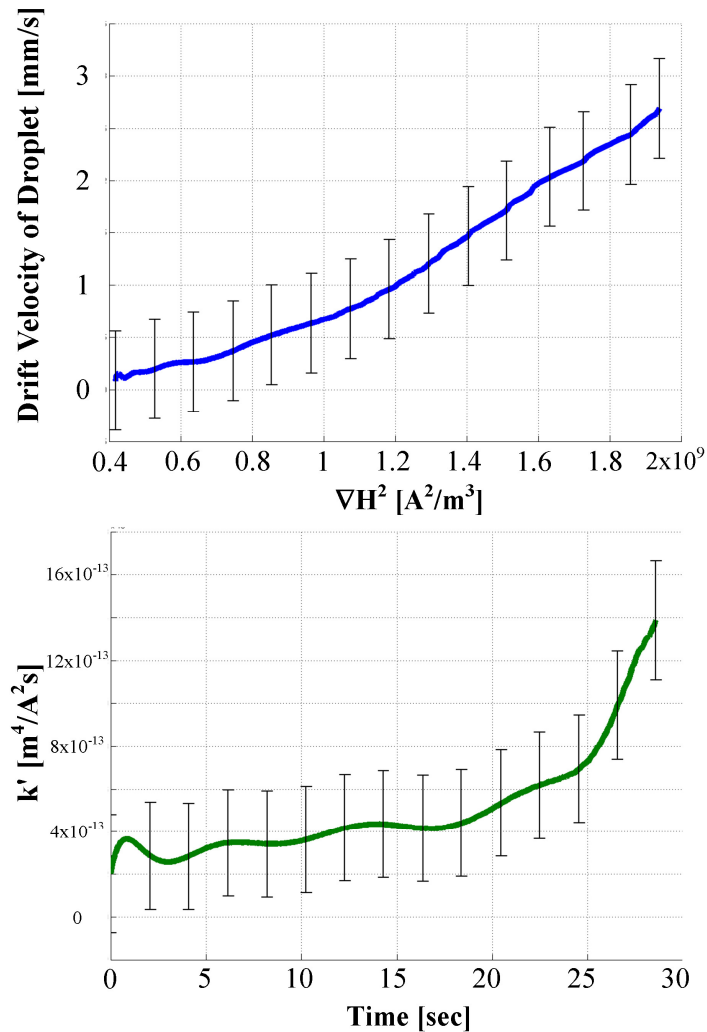


Figure SM-5: Inferring the instantaneous k' value. (Top) The instantaneous drift velocity of the droplet and its associated local gradient of the magnetic intensity squared are plotted in blue. As the gradient of the magnetic intensity squared increases, so does the drift velocity. (Bottom) The resulting inferred time dependent k' value is plotted in green versus time. It can be seen that k' remains relatively constant until a sharp increase at 20 seconds. The error bars represent two standard deviations away from the measured value.

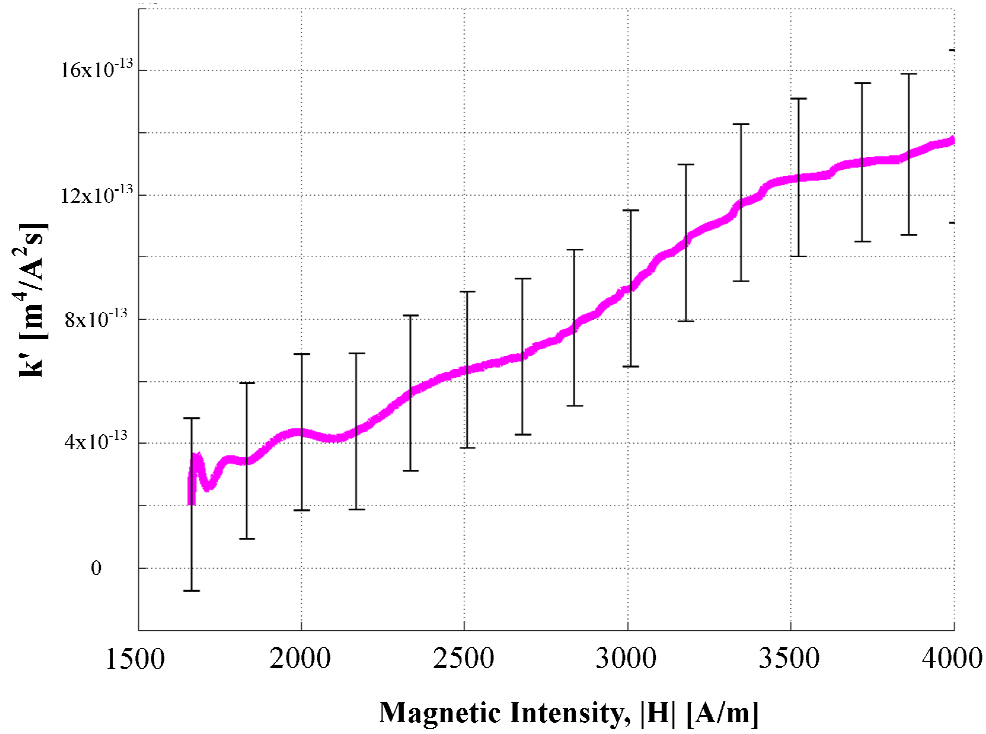


Figure SM-6: Dependence of k' on the local magnetic field intensity $|H|$. As the magnetic intensity increases, the k' value also increases.

As mentioned in Section **Error! Reference source not found.**, to qualitatively understand the above k' behavior we considered four possible scenarios for nano-particle interactions within a moving droplet. These included: 1) the independent motion of a single nano-particle, 2) the motion of a chain of particles held together by magnetic particle-to-particle interactions, 3) the motion of an agglomerate of particles held together by magnetic particle-to-particle and chain-to-chain interactions, and 4) the motion of a rigid ferromagnetic bead the size of the droplet. Table SM-1 shows the parameters for each possible scenario. The table lists the normalized drag force (force per unit velocity) and the normalized magnetic force (force per gradient of the magnetic field squared) for each of the four cases. Here the net magnetic force is computed by simply summing up the magnetic forces on each particle in the aggregate. The drag force is computed by the appropriate Stokes drag for a cylinder [6] (shape approximation for option 2) or a sphere [2, 3, 7] (a shape approximation for option 3).

At the equilibrium velocity, which the droplet achieves quickly, the net magnetic force equals the net opposing viscous drag force ($F_M = F_D$) thus ensuring that the k' as defined in the table matches the k' in equation **Error! Reference source not found.** It is immediately clear from Figure SM-4 and the table that cases 1 and 4 serve as an upper and lower bound for the motion of the droplet – the first severely under-predicts the motion (a single nano-particle will barely move under the applied magnetic force) and a rigid droplet over-predicts it (assuming that all the nano-particles are effectively held together rigidly is not true). Option 2 also under-predicts the motion

since, even if the chain of nano-particles is the length of the entire droplet, the resulting net magnetic force on the chain is still not large enough to sufficiently overcome viscous drag and create a k' of the needed magnitude. This only leaves option 3 as a possibility.

Table SM-1: The four considered scenarios with the parameter values for each case are shown. The Stokes drag force divided by the drift velocity [kg/s], a magnetic force divided by the gradient of the magnetic intensity squared [kg m⁴/A² s], and the k' coefficient [m⁴/A² s]. It is clear that options 1 and 2, even if the length of the chain is the entire length of the droplet, have a maximum k' value much smaller than the needed $k' \sim 3 \times 10^{-13}$ value. Scenario 4 has a k' that is too great. Scenario 3 can produce the desired k' value for agglomerates that have a radius 22% of the radius of the entire ferrofluid droplet (each such agglomerate would contain approximately 1% of the droplets total number of nano-particles).

	Normalized Drag Force (F_D / v)	Normalized Magnetic Force ($F_M / \nabla H^2$)	$k' = \frac{F_M / \nabla H^2}{(F_D / v)}$
1) Single particle	5.4×10^{-8}	8.5×10^{-28}	1.5×10^{-20}
2) Max chain of particles	7.7×10^{-5}	1.8×10^{-23}	2.4×10^{-19}
3) Agglomerate of particles (22% size of droplet)	2.5×10^{-4}	8.7×10^{-17}	3.5×10^{-13}
4) Rigid droplet	1.2×10^{-3}	8×10^{-15}	7×10^{-12}

Option 3 is consistent with the results reported in [3, 7] and can produce a k' of the needed magnitude. It implies that if, on average, nano-particles in the ferrofluid droplet agglomerate into clumps that each contain approximately 1% of the nano-particles in the droplet, then, as these clumps move under the action of the magnetic field and are opposed by a viscous drag per clump, the resulting motion will give a k' of the observed magnitude.

4. References

1. Rosensweig, R.E., *Ferrohydrodynamics*. 1985, Mineola, NY: Dover Publications, Inc.
2. Zubarev, A.Y., S. Odenbach, and J. Fleischer, *Rheological properties of dense ferrofluids. Effect of chain-like aggregates*. Journal of magnetism and magnetic materials, 2002. **252**: p. 241-243.
3. Wu, M., et al., *Magnetic field-assisted hydrothermal growth of chain-like nanostructure of magnetite*. Chemical Physics Letters, 2005. **401**(4-6): p. 374-379.
4. Mendeleev, V.S. and A.O. Ivanov, *Ferrofluid aggregation in chains under the influence of a magnetic field*. Physical Review E, 2004. **70**(5): p. 51502.
5. Wang, Z. and C. Holm, *Structure and magnetic properties of polydisperse ferrofluids: A molecular dynamics study*. Physical Review E, 2003. **68**(4): p. 41401.
6. Ui, T.J., R.G. Hussey, and R.P. Roger, *Stokes drag on a cylinder in axial motion*. Physics of Fluids, 1984. **27**: p. 787.
7. Odenbach, S., *Magnetoviscous Effects in Ferrofluids*. 2002: Springer.